ABSTRACT

Title of Document: OPTIMIZATION AND IMPLEMENTATION OF A THERMOACOUSTIC FLASHOVER DETECTOR

Kenneth A Hamburger
Master of Science, 2013

Directed By: Peter Sunderland, Associate Professor
Marino di Marzo, Professor
Department of Fire Protection Engineering

The thermoacoustic flashover detector is to be a helmet-mounted device that responds to deteriorating conditions in a compartment fire and produces an audible alarm to alert emergency personnel in time for an escape or change in tactics. An operational prototype device was designed at University of Maryland in 2011, and featured an aluminum, copper, and MACOR tube 178 mm long and 25.4 mm in diameter. The prototype was powered by an external heat band, which provided 44 watts of power at $308^{\circ}C$. Optimization of the prototype is conducted across several parameters including power consumption and temperature gradient. To that end, two scaled-down models of diameters 22 mm and 17 mm are constructed, both of which fail to produce sustained sound. Adding water to the device reduces the onset power consumption to 22 watts and the maximum temperature to $285^{\circ}C$, which represents the most efficient prototype of the device. A system of radiant heat collector panels and copper-water heat pipes is designed to replace the external heat band as a power source. A heat transfer analysis is conducted to determine the necessary size of the collector panels for proper activation, as well as the response time of the system. Total required surface area will depend on future design parameters, but reasonable estimates suggest that it will be between $0.02-0.03m^2$. An acoustic analysis of the optimized device is conducted, revealing a fundamental frequency of 500Hz at 101 dB.

OPTIMIZATION AND IMPLEMENTATION OF A THERMOACOUSTIC FLASHOVER DETECTOR

By
Kenneth A Hamburger

Thesis submitted to the Faculty of the Graduate School of the
University of Maryland, College Park, in partial fulfillment
of the requirements for the degree of
Master of Science
2013

Advisory Committee:
Associate Professor Peter Sunderland, Chair
Professor Marino di Marzo
Professor Emeritus James G. Quintiere

LIST OF TABLES

LIST OF FIGURES

NOMENCLATURE

Roman Letters

A	Contact surface area
C	Constant of integration
c	Specific heat
d	Diameter of heat pipe
e	Euler's number
h	Heat transfer coefficient
K	Liquid-wick resistance factor
k	Thermal conduction coefficient
L	Length of thermoacoustic device
l	Length of collector plate / resistance path length
m	Mass
n	Quantity (integer)
Q	Symbolic differential operator
$\dot{q}$	Power
R	Resistance
T	Temperature
t	Time
w	Width of collector plate
x	Physical distance from closed end / heat pipe

Greek Letters

β	Symbolic differential operator
Δ	Difference
δ	Thickness of collector plate
ε	Emissivity
θ	Symbolic differential operator
π	Pi
ρ	Density
σ	Stefan-Boltzmann constant
τ	Time constant
ϕ	Symbolic differential operator

Subscripts

adiabatic	Relating to the adiabatic section of the heatpipe
c	Convective
collector – heatpipe	Relating to the collector-heatpipe interface
heatpipe – axial	Relating to the axial resistance of the heatpipe
heatpipe – liquidwick	Relating to the liquid-wick resistance of the heatpipe

HP	Located on the cold end of the heat pipe
i	Inner
l	Loss / liquid
o	Outer
pipes	Relating to the heat pipes
r	Radiative
stack	Relating to the stack
w	Wick
∞	Ambient
0	Located at the base of the collector

1 Introduction

Firefighting is widely considered to be one of the more dangerous occupations in modern society. During routine suppression and rescue operations, firefighters are exposed to a variety of hazards, most notably the intense thermal energy from fire and smoke. Although the research and development behind firefighter protective clothing, suppression equipment, and firefighting tactics are constantly improving, fireground hazards continue to contribute to thousands of preventable injuries and deaths each year. The National Fire Protection Association estimates that in 2011, 70,090 firefighters were injured in the line of duty in the U.S., 30,505 of which occurred during fireground operations. [1] Additionally, 2011 saw 61 on-duty fire deaths in the U.S. [2]

One hazard of particular interest is an enclosure fire phenomenon known as "flashover." Flashover, in layman's terms, is the transition between a fire in a room and a room on fire. Flashover is typically accompanied by incident heat fluxes in excess of $20 {kW}/{m^2}$ and temperatures in excess of $500^{\circ}C$. [3] These heat fluxes and temperatures are sufficient to degrade firefighting protective gear and melt face masks in relatively short periods of time, and therefore present great danger to firefighters operating in such environments. [4] To compound the thermal hazards, flashover can often occur quickly and without discernable warning. Diminished sensation and visibility due to efficient firefighting protective gear and thick smoke can often obscure the onset of flashover, and leave a firefighter with insufficient time to escape a dangerous environment.

The goal of the thermoacoustic flashover detector project is to design a passive, helmet-mounted device that will issue an audible warning to alert firefighters of impending flashover, and allow them sufficient time to escape from a deteriorating environment. The device is designed to operate without batteries, electricity, or moving parts, and use only radiant heat from the device's environment to generate a sound wave. It is the hope of the researchers that the advanced warning provided by the thermoacoustic flashover detector will allow for increased situational awareness during fireground operations, which will, in turn, lead to decreased frequency of injury and death due to the hazards associated with flashover.

The research presented here details the optimization of a prototype device, initially designed by Buda-Ortins, [5] for various parameters including input temperature, input power, size, simplicity, and cost. Additionally, a steady-state heat transfer model is developed, which details the mechanics of the heat transfer from the smoke layer to a system of "collector" panels, and then on to the device itself. The heat transfer model is accompanied by a transient analysis, which aims to predict the response time of the alarm. Lastly, an analysis of the sound output of the device is conducted to determine the practicality of the alarm with regard to sound volume and frequency.

1.1 Flashover

Enclosure fires can be divided into stages in terms of compartment temperature development. The five stages most commonly listed are: ignition, growth, flashover, fully developed fire, and decay. [3] The temperature development through these stages is depicted graphically in *Figure 1-1*.

Figure 1-1: Temperature variation with time in an enclosure fire. [3]

Ignition is the process that initiates an exothermic reaction, and can either be piloted or spontaneous. Following ignition, the fire experiences a growth stage, which can occur in several different ways depending on the type and geometry of fuel, access to oxygen, and interaction with surroundings. In smoldering fires, the energy release rate may stay relatively low throughout the growth period, even while toxic gasses are being produced. The growth period of a smoldering fire may be very long, and such a fire may die out before subsequent stages are reached. Flaming combustion typically experiences a more rapid growth period, where the

flame heat flux is sufficient to cause flame spread across the fuel surface and ignite adjacent fuel packages. The growth stage is also dependent on the availability of oxygen; a dearth of oxygen can limit the growth and spread of an incipient fire.

During the growth phase, an extremely hot and radiant smoke layer begins to form near the ceiling. As the fire continues to release its own thermal energy, the smoke layer begins to irradiate all the contents of the enclosure. The ultimate effect of these combined heat fluxes is the imprecisely defined transition point known as flashover. Flashover is defined and described in a variety of ways. Some definitions are qualitative, and refer to it as the point in growth of a flaming fire where the flames are no longer confined to burning items, but also occur at locations remote from the seat of the fire and in the fire effluent. Another qualitative definition offered by the International Standards Organization is "the rapid transition to a stage of total surface involvement in a fire of combustible material within an enclosure." [6] Quantitative descriptions of flashover typically include floor-level heat flux and temperature values in the area of $20 \, {}^{kW}/_{m^2}$ and $500^{\circ}C$ respectively. Despite the varying descriptions and definitions of flashover, several commonalities pervade: flashover is accompanied by a drastic increase in heat flux and temperature, and can occur very suddenly—as fast as 20 seconds, in some cases. [3] The high temperatures and heat fluxes pose an enormous hazard to firefighters operating inside the fire compartment; firefighter protective clothing is not capable of withstanding flashover-level thermal insult. In addition to the degradation of the protective materials, the Lexan (polycarbonate) face shield and plastic air regulator become susceptible to melting. The high temperatures may also weaken structural

components and increase the likelihood of collapse. Apart from the severity of flashover, the potential suddenness with which it can occur compounds the danger to compartment inhabitants; without sufficient notice of impending flashover, escape becomes impossible. For these reasons, flashover is usually lethal to all compartment occupants.

Flashover is followed by the fully developed stage of fire. During this stage, the energy release rate of the fire is at its greatest. The fully developed compartment fire is often limited by the amount of available oxygen, and it is during this stage that flames display oxygen-seeking behavior such as shooting out of windows or doors. As the fuel is consumed, the fire enters the decay stage, and the energy release rate begins to diminish. This stage may also see the fire revert to fuel-limited combustion, depending on the geometry of the room and ventilation openings. The decay phase continues until no more fuel is available to burn, at which point the fire becomes extinct. [3]

1.2 Thermoacoustics

Thermoacoustics is a broad term that describes the intersection of the fields of thermodynamics and acoustics. When invoked as a mechanism of operation, thermoacoustics refers to the adiabatic expansion and compression cycles of gas parcels, known as compressions and rarefactions, within a cavity and resultant sound waves. Devices that operate on thermoacoustic mechanisms can be divided into two classes: standing wave devices and traveling wave devices. Each of these classes can be further subdivided into two more classes: engines (or prime movers) and heat pumps. [7]

A traveling wave is a wave that propagates as a periodic function of space and time. An example of a traveling wave is a flashlight shining on a wall; the light moves through space and time with a characteristic frequency and wavelength until it hits the wall and is converted to other forms of energy. A standing wave results from a medium moving in a direction opposite to the wave, or more commonly, interference between waves traveling in opposite directions. When the superposition of the interfering wave is considered, the resulting wave appears to be standing still; a perfect standing wave is only a function of space. Standing wave phenomena are fundamental to the operation of many musical instruments, and are studied in most introductory physics courses. One of the important properties of standing waves is that they can only take on certain frequencies, known as normal modes. The boundary conditions of the cavity (open/closed) dictate pressure nodes or antinodes, and therefore only frequencies and wavelengths that meet those constraints are allowed. [8] The first two standing wave modes (m=1, and m=2) are shown for three different boundary conditions in *Figure 1-2*. The blue lines represent displacement of the medium, and the red lines represent pressure variations. Where the tube is closed to the atmosphere, there is always a pressure antinode and a displacement node. Where the tube is open to the environment, there is always a pressure node and a displacement antinode. Of particular interest is the closed-open boundary condition; where closed-closed and open-open boundary conditions contain *m* half-wavelength segments, the closed-open tube contains 2*m-1* quarter-wavelength segments. Therefore, the normal frequencies of

the closed-open tube are half the normal frequencies of the closed-closed and open-open tubes.

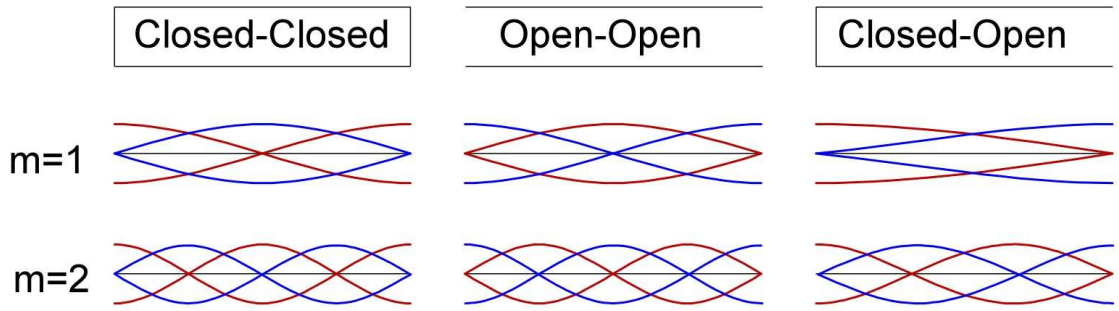

Figure 1-2: The first two normal modes for various boundary conditions. Blue lines represent medium displacement and red lines represent pressure variations.

Thermoacoustic engines, also known as prime movers, use a temperature gradient to produce high-amplitude sound waves. Thermoacoustic devices can also be run in reverse; heat pumps use sound waves to pump heat from one place to another. Cooling is the most common application for thermoacoustic heat pumps, and for that reason they are also known as thermoacoustic refrigerators. [7] The components common to all thermoacoustic devices are a hot heat exchanger, a cold heat exchanger, a resonator, and a stack (standing wave) or regenerator (traveling wave). The hot heat exchanger is the site where heat is supplied in the case of an engine, or removed in the case of a heat pump. Conversely, the cold heat exchanger is the site where heat is removed in the case of an engine, and the source of cooling in the case of a refrigerator. Between the heat exchangers is a stack. Stacks are components consisting of small parallel channels, and are the locations where the actual conversion of heat to work (or vice versa) takes place. The resonator is simply a hollow extension of the cavity. A typical arrangement of these parts for a standing wave engine is shown in *Figure 1-3.*

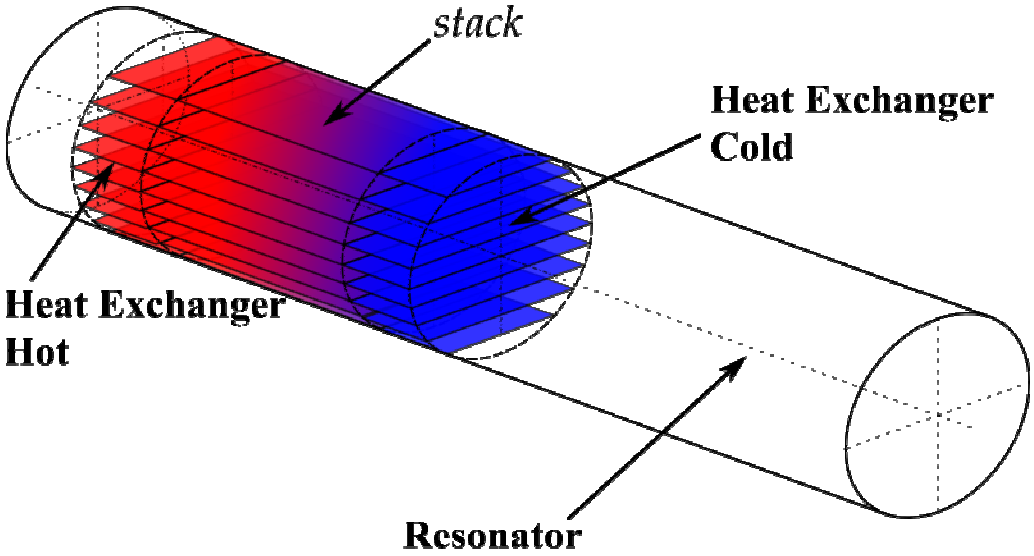

Figure 1-3: The components and arrangement of a typical standing wave thermoacoustic engine. [9]

The physical mechanism by which the stack converts a temperature gradient to an acoustic wave in an engine is through cycles of compressions and rarefactions. Gas parcels in the hot half of the stack are cooler than their surroundings, and absorb heat from the hot heat exchanger. As the gas parcels heat up, they expand in the high-pressure zone surrounding the hot heat exchanger. The gas parcels move along the pressure gradient towards the cold heat exchanger, which is surrounded by a low-pressure zone. Here, the gas parcels are warmer than their surroundings, so they reject heat to the cold heat exchanger. This causes the gas parcels to contract in the low-pressure zone. This is the essence of the work produced by the gas in the stack: expansion when pressure is high and contraction when pressure is low. In this way, the stack pumps acoustic power into the standing wave. In coupled oscillations, the standing wave provides the oscillating pressure and motion that causes the gas parcels to experience the oscillating temperature responsible for the compressions and rarefactions.

1.3 Review of Example Models

Several preexisting thermoacoustic engines were used as a foundation for the construction of a prototype model. These models provided insight into the device's approximate dimensions, materials, methods of heat input, methods of cooling, orientation, and assembly. The four groups of investigators that were most influential in the design of the prototype device were Jung and Matveev [10], Wheatley et al. [11], Symko et al. [12], and Smoker et al. [14]

Jung and Mateev's experimental model, shown in *Figure 1-4,* consisted of a flanged copper cap, ceramic stack holder, copper fitting for a pressure transducer, and a flanged copper tube open on both ends. To ensure airtight seals, graphite gaskets were used at the junctions, and bolts were placed through the flanges to compress the device. Heat exchangers, which are not clearly shown in the figure, consisted of two layers of copper mesh on either side of the stack, which was composed of reticulated vitreous carbon. To establish a temperature gradient across the stack, a heat band was used to heat the hot side, and a cooling jacket using flowing water-cooled the cold side. Jung and Matveev conducted several tests using differently sized tubes for the open end. Among their important findings was that a stack placement of $x_{stack}/L = 0.18$ and $x_{stack}/L = 0.07$ corresponded to the smallest measured temperature gradient in the stack. [10]

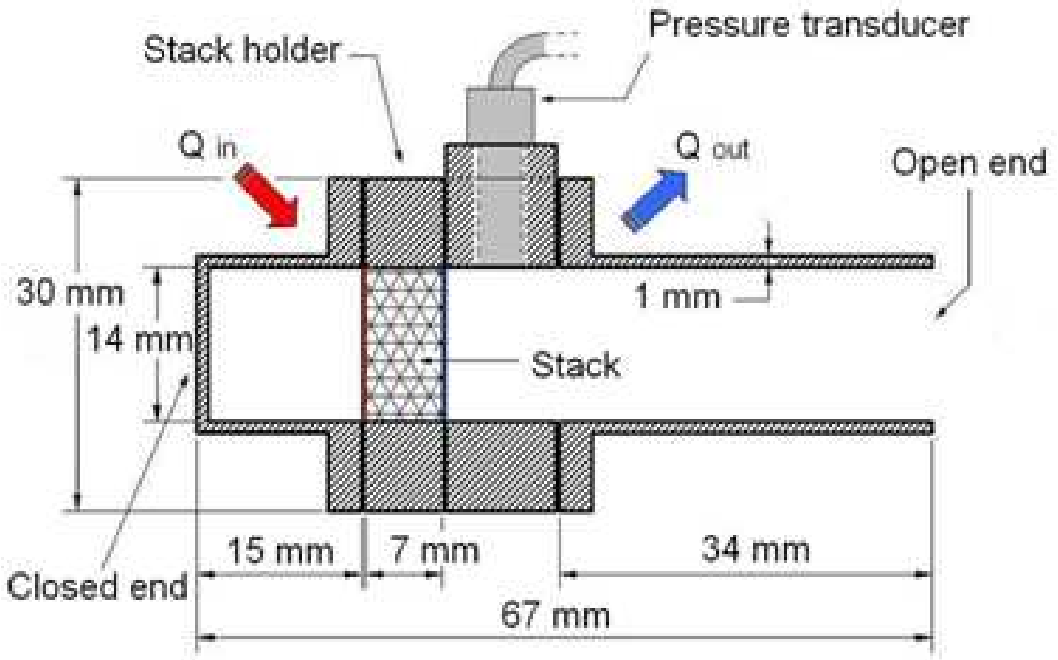

Figure 1-4: Thermoacoustic engine designed by Jung and Matveev. [10]

Wheatley, Hofler, Swift, and Migliori used a different approach; rather than supply heat to the hot end, they cooled the cold end with liquid nitrogen, and left the hot end at ambient temperatures. Their design used closed-open and open-open copper tubes for the ends of the device, but the stack holder was mode from poorly conducting stainless steel, and the stack itself was composed of fiberglass plates. Copper strips across the ends of the stack holder served as heat exchangers. Brass flanges held the parts together. Unlike the other designs, the stack holder was placed in the center of the device, or $x_{stack}/L = 0.5$. The open end of the tube was immersed in liquid nitrogen and upon removal, resonated at 200 kHz. The temperature gradient across the stack was estimated to be $216^{\circ}C$. [11] The importance of this design is its illustration that absolute temperatures matter little, if at all; the critical parameter for the proper operation of a thermoacoustic engine is the temperature gradient.

Symko designed several thermoacoustic resonators on a smaller scale, with devices in the 2 to 4 cm range. These devices used cotton or glass wool for stack materials and a copper mesh for heat exchangers. [12] Of particular interest is a 38 cm-long prototype designed by one of Symko's partners featuring a temperature gradient of only $32^{\circ}C$ and power requirement of 2 W. [13] This accomplishment indicates the potential that scaling thermoacoustic devices holds for reducing temperature and power requirements. Another one of Symko's colleagues demonstrated that effects of air pressure on the necessary temperature gradient; namely, increasing the air pressure allowed for reducing the temperature difference across the stack to as low as $25^{\circ}C$.

The last example model, and the most germane to the project at hand, is that of Smoker, Nouh, Aldraihem, and Baz. [14] In the course of their research on energy harvesting, Smoker et al. designed a thermoacoustic engine made from Pyrex glass. Instead of heat exchangers, a resistance wire with a DC power supply was zig-zagged across the inside of the tube, and no cold heat exchanger was present. The overall length of the device was 175 mm and the internal diameter was 20 mm. The stack position was $x_{stack} = 64mm$, or $x_{stack}/L = 0.37$. This device produced a 500 Hz tone at 122 dB with a power input of 33W. [14] For more information on how the initial prototype was designed, see *Prototype Design for Thermoacoustic Flashover Detector.* [5]

2 Overview of Work by Buda-Ortins

Much of the research contained herein is based on work done by Buda-Ortins, and outlined in her Master's thesis. [5] Buda-Ortins' major accomplishments were constructing a working prototype of a thermoacoustic whistle powered solely by heat, measuring the temperature profile inside the device, measuring the response time of the whistle, and measuring the volume and frequency of the sound output. Other accomplishments include the implementation of a unique material, "copper foam," to effect heat transfer within the device, and a system of seals that ensured air-tightness, but also allowed for easy assembly and disassembly of the prototypes.

The relevant quantitative results of Buda-Ortins' research are outlined here:

- 178 mm long thermoacoustic whistle, whose design is detailed in the next section: *Overview of Prototype Device*.
- Sound onset achieved with 44W of power, provided by an electrically powered heat band.
- Heat band temperature of $308^{\circ}C$, and ΔT across the stack of $191^{\circ}C$ to achieve sound onset.
- Continued sound (after onset) achieved with 34W of power, provided by an electrically powered heat band.
- Heat band temperature of $295^{\circ}C$ and ΔT across the stack of $146^{\circ}C$ to maintain sound after onset.

3 Overview of Prototype Device

The prototype devised by Buda-Ortins, and starting point for optimization work is shown in *Figure 3-1* and diagrammed in *Figure 3-2.*

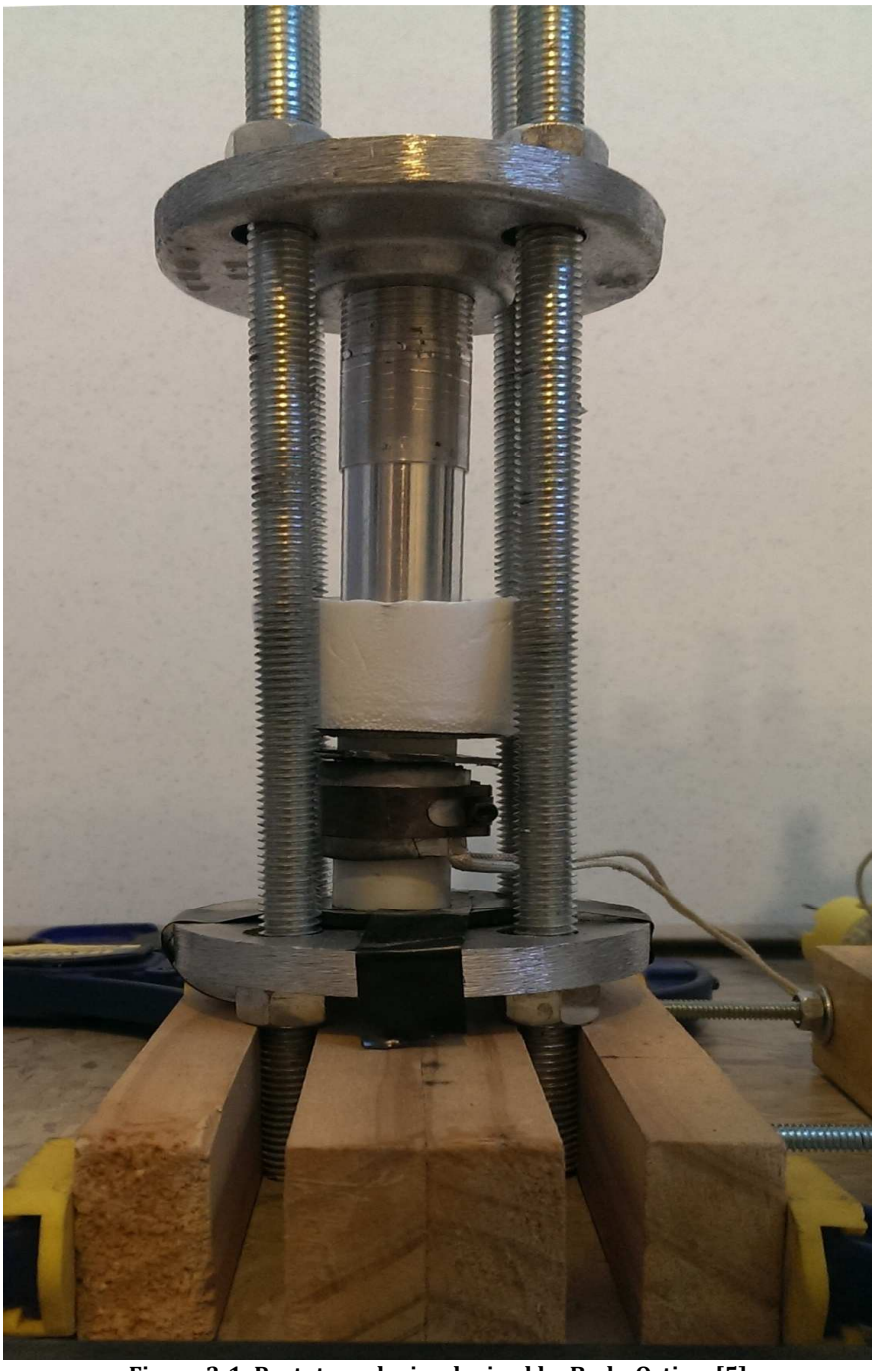

Figure 3-1: Prototype device devised by Buda-Ortins. [5]

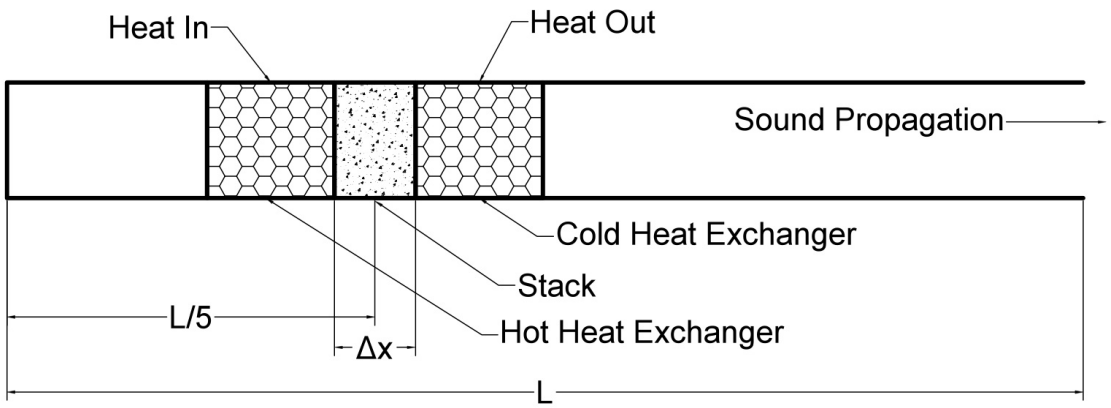

Figure 3-2: Prototype device devised by Buda-Ortins [5].

The dimensions and materials of each piece from left to right are given in *Table 3-1* below:

Piece	Length (mm)	Inner Diameter (mm)	Outer Diameter (mm)	Material
End Cap (Left)	31.8	20.3	25.4	MACOR
Hot Heat Exchanger	25.4	22.4	25.4	Copper Foam
Stack Holder	6.4	20.3	25.4	MACOR
Cold Heat Exchanger	25.4	22.4	25.4	Copper Foam
Resonator (Right)	88.9	20.3	25.4	Aluminum

Table 3-1: Dimensions and material of components in prototype device accurate to +/- 0.05mm.

The MACOR and aluminum pieces were all designed with small lips on their interior ends to ensure that the pieces would fit into one another and remain properly seated. The stack was comprised of loosely rolled steel wool, with an approximate density of $150\,{}^{kg}\!/_{m^3}$. At each junction, a graphite gasket of ${}^{1}\!/_{32}"$ thickness was placed around the lip of the MACOR/aluminum component to ensure that when axially compressed, the device was air-tight everywhere but at the open end. Axial compression was achieved with externally placed flanges and bolts mounted on a wooden base.

The copper foam used for the heat exchangers was procured from ERG Aerospace, and was chosen for its unique heat transfer properties. Officially titled Duocel® Copper Foam Alloy C10100, copper foam is a rigid, highly porous, and permeable structure of copper, which forms a three-dimensional array of honeycomb-like cells. Copper foam can be specified by two independent characteristics: relative density and pore size. Relative density is a measure of the copper foam's density compared to the density of a solid block of copper of the same volumetric dimensions. Pore size is specified in units of pores per inch (PPI) and represents the average number of cells per linear inch of foam in any direction within the lattice. The copper foam used in the prototype device had 20 pores per inch (20 PPI) and 8-12% relative density [15]. The high surface-area-to-volume ratio that copper foam provides is ideal for a heat exchanger of limited size; copper foam provides nearly ten times more surface area than a simple copper tube. The heat transferred through the process of convection, the dominant mode of heat transfer between the inner surface of the heat exchanger and the gas parcels, is directly proportional to the area of contact, so a large surface area inside the heat exchangers is critical to reduce resistance and maximize efficiency. For use in the prototype device, copper foam was attached to a hollow copper tube of wall thickness 3 mm by hydrogen brazing. Throughout the prototyping process, other materials and configurations were used as heat exchangers without success; only the copper foam heat exchangers allowed for the successful propagation of sound.

The stack holder was machined out of MACOR, but the stack itself is a piece of steel wool that sits inside the stack holder, with both ends in contact with the adjacent heat exchangers. The steel wool was standard, commercially available steel wool with fiber thickness $0.08-0.11mm$. The density of the steel wool in the stack holder could be varied by stuffing more or less steel wool into the cavity. The approximate density of steel wool that yielded the best results was $150 kg/m^3$. Using less steel wool often resulted in loss of contact with the heat exchangers and resulting temperature gradient. Using more seemed to inhibit airflow through the stack, and produced little or no sound.

4 Optimization Parameters

The prototype device was a valuable proof-of-concept and starting point for the ultimate goal of implementing a flashover alarm into firefighter helmets. For a variety of reasons, however, the device required optimization and refinement towards that end. The parameters selected for optimization were temperature, power consumption, device complexity, and as a practical consideration, cost. The prototype device produced sound only at temperatures above $300^{\circ}C$ in the hot heat exchanger. Temperatures in this range present several problems, but most importantly, this temperature range may simply not be feasible; the radiant smoke layer may not be capable of producing such high temperatures. Additionally, if the device is to be helmet-mounted, a piece of metal in this temperature range is dangerous to place so near a firefighter's head. Although the prototype's power consumption was not necessarily problematic, reducing the amount of power required for sustained sound propagation can only serve to improve the response time of the device, reduce the size and complexity of the energy collection apparatus, and ensure that the pre-flashover environment can activate the device. The complexity of the device is inherently minimal; the specifications of the project exclude batteries, electricity, moving parts, and components that require frequent replacement. Despite this, the device could benefit from further simplification. There are four junctions that require airtight seals, fragile MACOR lips that are susceptible to damage, and the expensive incorporation of the exotic copper foam, all of which diminish the durability and simplicity of the device. To improve the

design of the device with respect to these parameters, several modifications were attempted, the details and results of which are the subject of the following sections.

4.1 Eliminating Cold Heat Exchanger

The first and easiest modification to the prototype was the removal of the cold heat exchanger. The structure of the whistle contains some inherent cooling features without need of a heat exchanger; the aluminum resonating chamber acts as a heat sink on the cold end of the device, and the open mouth facilitates some air exchange with the ambient environment. The benefits of removing a heat exchanger are manifold: one of the four gasket seals is eliminated, increasing the reliability of the device and its ease of assembly. Furthermore, the copper foam of the heat exchangers is the most expensive component of the device; eliminating one of the two heat exchangers can significantly lower the total cost of the device.

Several attempts at producing sound with the modified device were made. In one design, the heat exchanger was removed and the aluminum resonating chamber was joined directly to the stack holder, as shown in *Figure 4-1.* In another design, the heat exchanger was replaced with a hollow copper cylinder to maintain the overall length of the whistle. In a third design, a Styrofoam cup full of water placed around the resonating chamber was used to enhance cooling on the cold end of the stack. Each design was tested multiple times with several steel wool densities in the stack holder ranging from $\sim 120 \, kg/m^3$ to $\sim 180 \, kg/m^3$. Each design was also assembled several times with fresh gaskets to ensure that air tightness was not the cause of failure.

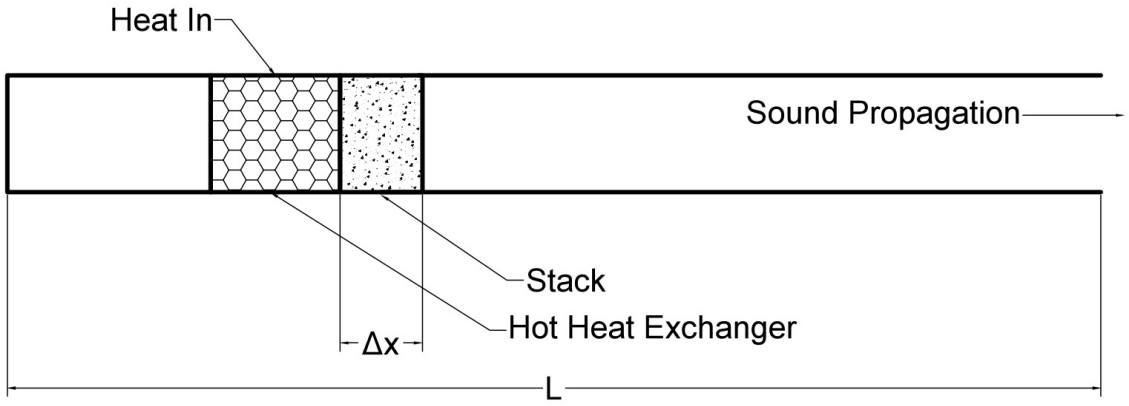

Figure 4-1: General design of one of several modified designs with the cold heat exchanger removed.

Each change in design unavoidably changed several characteristics of the device. Because all components of the whistle were custom machined, it proved difficult or impossible to redesign the whistle exactly as desired. For example, when the heat exchanger was removed, a longer resonating chamber would have been ideal to maintain the overall length of the device but was unavailable due to time constraints. The inadvertent changes that result from the design modifications created enormous difficulty in pinpointing the exact cause of failure. The suspected cause of failure is the lower temperature gradient on the cold side of the stack. Recall that the source of acoustic power is the compressive action that takes place in the low-pressure zone to the right of the stack. When a cold heat exchanger abutting the stack holder is present, the compressions take place immediately in both space and time. When a cold heat exchanger is absent, the compressions must take place over a much larger area that extends well into the resonating chamber and over a greater period of time. This reduces the amount of power available for driving the acoustic oscillations, as well as interferes with the cyclical flow of gas parcels.

4.2 Reducing Internal Diameter

The purpose of creating prototypes with reduced diameters is to reduce the temperature and energy input requirements. With all other proportions remaining constant, a smaller diameter yields a smaller volume in each component, and a smaller number of gas parcels that drive the oscillations. A smaller number of gas parcels require less net energy to force their compressions and rarefactions, and it was hoped that these scaled prototypes might produce a sound comparable to the original prototype with less energy and at a lower temperature.

Modifications to reduce diameter proved significantly more elaborate than the first set of modifications, and were conducted in two stages. The first stage was an attempt to scale down the internal diameter of the MACOR and aluminum pieces, but leave the copper foam heat exchangers unchanged. The general design of this prototype is shown in *Figure 4-2.* This stage was an intermediate attempt to scale down the device without purchasing new copper foam heat exchangers, which are costly and take several months to prepare. The complete list of parts used in this intermediate prototype is shown in *Table 4-1.*

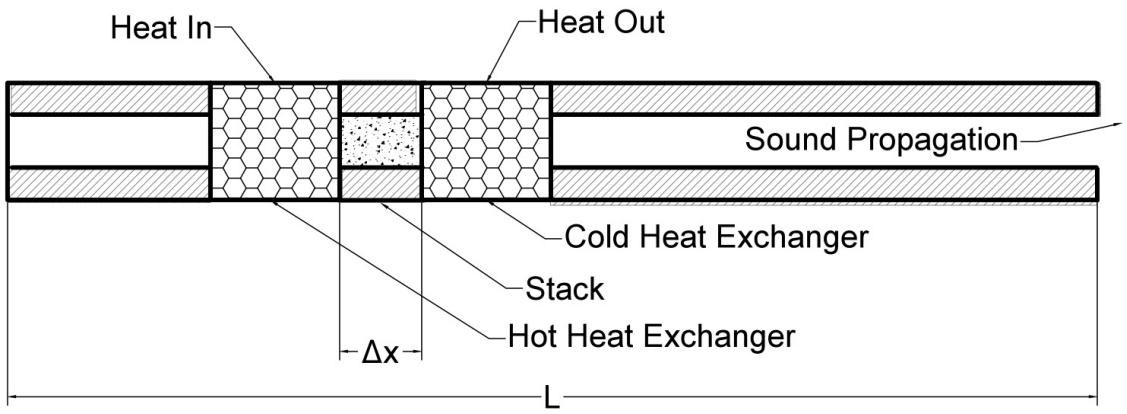

Figure 4-2: Diagram of prototype with existing heat exchangers and MACOR parts of decreased diameter.

Piece	Length (mm)	Inner Diameter (mm)	Outer Diameter (mm)	Material
End Cap (Left)	31.8		25.4	MACOR
Hot Heat Exchanger	25.4	22.4	25.4	Copper Foam
Stack Holder	6.4		25.4	MACOR
Cold Heat Exchanger	25.4	22.4	25.4	Copper Foam
Resonator (Right)	88.9		25.4	Aluminum

Table 4-1: Dimensions and material of components in prototype device accurate to +/- 0.05mm.

The modified prototype failed to produce any sound. The device was deconstructed and reconstructed several times in order to rule out problems with the assembly of the device. Graphite seals were replaced, the amount of axial compression was varied, the stack density was varied, and the heat input was varied, all to no effect. As with the first modified prototype, it was difficult to pinpoint the exact cause of failure. One possible explanation is the impact that a non-uniform diameter might have on the cyclical movement of gas parcels. In a device of uniform internal diameter, changes in gas temperature and pressure result in a net axial movement. In a device of non-uniform diameter, the gas has the opportunity to move in the radial direction when it is passed from a tube of one diameter to a tube of another. Radial transport of the gas parcels may be enough to prevent the establishment of a sustainable cycle of motion, which then precludes audible resonation.

The failure of the partially scaled model to produce sound prompted the second stage of modifications: the production of reduced scale models with heat exchangers or matching internal diameter. To that end, two different complete

prototypes were designed and constructed. Where the original prototype had an external diameter of 25.4 mm, the second and third prototypes had external diameters of 22 and 17 mm, respectively. The complete list of parts used in the second and third prototypes are shown in *Tables 4-2 and 4-3.*

Piece	Length (mm)	Inner Diameter (mm)	Outer Diameter (mm)	Material
End Cap (Left)	31.8	17	22	MACOR
Hot Heat Exchanger	25.4	19	22	Copper Foam
Stack Holder	6.4	17	22	MACOR
Cold Heat Exchanger	25.4	19	22	Copper Foam
Resonator (Right)	88.9	17	22	Aluminum

Table 4-2: Dimensions and material of components in prototype device accurate to +/- 0.05mm.

Piece	Length (mm)	Inner Diameter (mm)	Outer Diameter (mm)	Material
End Cap (Left)	31.8	12	17	MACOR
Hot Heat Exchanger	25.4	14	17	Copper Foam
Stack Holder	6.4	12	17	MACOR
Cold Heat Exchanger	25.4	14	17	Copper Foam
Resonator (Right)	88.9	12	17	Aluminum

Table 4-3: Dimensions and material of components in prototype device accurate to +/- 0.05mm.

Scaling the MACOR and aluminum pieces was simple; the new pieces were machined with smaller dimensions, but were otherwise identical to their full-sized counterparts. Scaling the copper foam proved a little bit more complicated. The purpose and importance of the copper foam lies in its heat transfer characteristics; specifically, its ability to conduct heat from the copper walls to the interior foam and then convect it to the surrounding gas. The scaling process affects both conduction

and convection. The copper foam is a three-dimensional mesh and occupies the volume bounded by the copper walls of the heat exchanger. When scaled, the external surface area varies with respect to the radius of the tube and the volume of the copper foam varies with respect to the square of the radius of the tube. It's unlikely that this would present a problem; if anything, more energy per unit volume will be available. The critical parameter for convection is the inner surface area of the heat exchanger in contact with the gas. A series of calculations (*Appendix A*) revealed that the presence of copper foam in the original prototype's heat exchangers increased the available interior surface area by a factor of about 7. When designing the smaller heat exchangers, the relative density and pore size of the heat exchangers were selected in such a way as to maintain the seven-fold increase in interior surface area. The 19 mm ID heat exchangers were ordered with 12% relative density and 40 pores-per-inch and the 14 mm ID heat exchangers were ordered with 6% relative density at 40 pores-per-inch. The devices were assembled in the same way as the original prototype using steel bolts and flanges to provide axial compression and graphite gaskets at each junction.

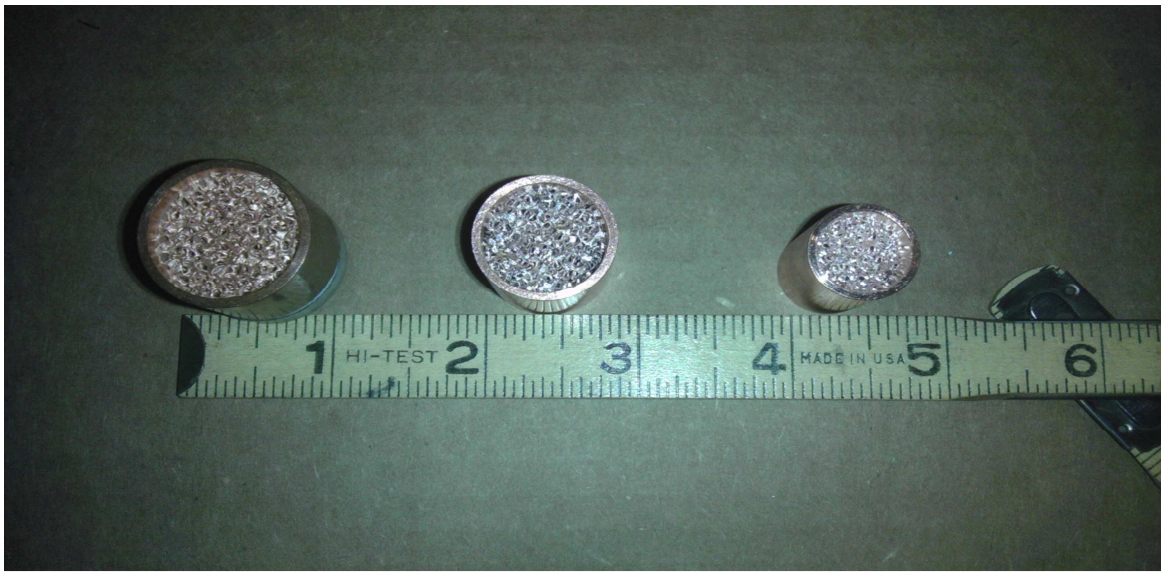

Figure 4-3: Copper foam heat exchangers in three sizes.


Figure 4-4: Exploded view of all three model's components in order of assembly.

The results of these scaled-down devices are slightly more informative than the previous model. While neither of the two smaller models produced sustained acoustic oscillations, the larger of the two did produce some effects similar to those seen in the full-size prototype. When the full-size prototype started reaching

temperatures near the onset temperature ($260^{\circ}C - 300^{\circ}C$) the device began to respond to external acoustic drivers. If the device's mouth was tapped or a loud sound was played near the opening, the device would resonate for a small amount of time and the resonations would die out. At $260^{\circ}C$, the resonations are almost imperceptible. Nearer to $300^{\circ}C$, the resonations lasted for 2-3 seconds before dying out. When the device reached its onset temperature, the externally induced resonations would give way to continuous, sustainable resonations that lasted until the device was cooled. The larger of the two smaller models displayed this ability to "carry" some resonance in the range $300^{\circ}C - 330^{\circ}C$, but was unable to produce indefinite sound even at the heat band's maximum temperature. The smaller of the two models did not display this ability, and made no sound at all.

A crude pattern of behavior emerges from these results. Where the full sized model "carried" sound between $260^{\circ}C - 300^{\circ}C$, the next largest did so between $300^{\circ}C - 330^{\circ}C$, and the smallest did not carry sound at all, suggesting that the temperature it requires is beyond the capacity of the heat band. As the size of the model shrinks, the minimum temperature (or temperature gradient) requirement increases. This is the opposite effect of what had been intended and expected. There are several possible explanations for this phenomenon, but no easy way to test them. One possible explanation is the change in the area-to-volume ratio inside the tube. While it was assumed that a greater area-to-volume ratio would benefit the operation of the device by providing more energy per unit volume, perhaps there a minimum temperature-to-energy ratio exists as well. With an abundance of energy available to the gas parcels, it stands to reason that they heat up and move

more quickly than the gas parcels in the original prototype. If the hot gas parcels reach the cold side of the heat exchanger before sufficient power can be transferred to the acoustic wave, the temperature gradient across the stack begins to suffer. Another possible explanation is that with smaller amounts of gas in the device, there is less temperature variation across the fluid both radially and axially. The resulting difference in fluid velocity profile could be detrimental to the establishment of an acoustic wave. Lastly, there exists the possibility that the friction of the walls or a viscous boundary layer inhibits the net motion of gas parcels. As the diameter shrinks, the amount of gas that is unaffected by the friction near the walls diminishes, until insufficient heat transfer remains to power the acoustic wave.

4.3 Addition of Water

The last modification was made by way of an accidental discovery. During experimentation with the original prototype, a small amount of water dripped into the open end of the tube. When the water hit the hot heat exchanger, it began to boil, letting off an audible hiss. The hissing quickly gave way to whistling at a temperature that was lower than previously thought to have been necessary. Thermocouple measurements revealed that the heat band temperature at the onset of whistling when water had been introduced to the device was at $285^{\circ}C$, $23^{\circ}C$ lower than the $308^{\circ}C$ that Buda-Ortins found when experimenting without water.

The operation of the device is far too complex to accurately assess what systems are affected by the presence of water and how they are affected. The major results that come from the incorporation of water are a slightly lower onset

temperature, and increased reliability. Increased reliability is measured qualitatively by the evenness of the sound; the whistle would occasionally fade in and out as the internal temperature fluctuated, but would do so less frequently when water was present. After 30-60 seconds, when the water had evaporated, the evenness of the sound began to diminish, although this may be due in part to the loss of a temperature gradient across the stack as the device reaches steady state. The causes of these changes in operation are likely due to the thermal properties of water. Without water, all gas parcel movement is driven by the expansion and contraction of air. When considering the ideal gas approximation for air, the volumetric changes vary in a near-linear fashion. When liquid water is vaporized, however, its volume expands by a factor of several hundred. This massive expansion amplifies the oscillatory motion of air, and serves to "seed" the oscillations similarly to the tapping of the opening to induce the initiation of self-sustaining oscillations.

5 Power Requirements

The temperature input across all the prototypes was found to be the lowest with the original model constructed by Buda-Ortins that incorporated the used of 1-2 mL of water. This model was therefore chosen for further analysis and used as a basis for the heat transfer model. The energy input to the device was measure by establishing a power curve for the heat band used to power the device. The heat band was connected to a Powerstat 3PM116B Variac, which allows a user to vary the voltage to an appliance between 0-120% of the variac input voltage (110V AC), with an accuracy of $\pm 5V$. Using a Sperry DSA-500 Ammeter, the amperage draw of the heat band was measured as the voltage was varied from 0-100% of the variac input voltage. Sound onset was measured as the point at which continuous audible sound emanated from the device. Once the device sounded, the voltage was slowly lowered (5V/min) until continuous sound ceased, marking the minimum amount of power to maintain resonation. The heat band's curve is shown in *Figure 5-1.*

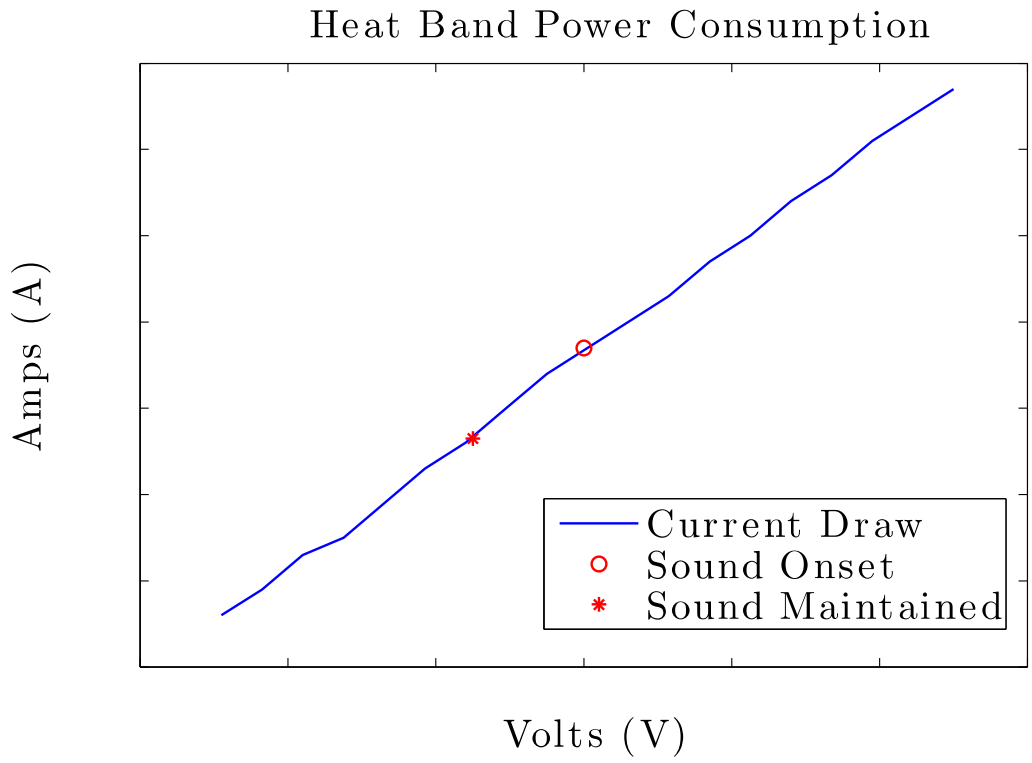

Figure 5-1: Amperage draw of heat band for varied voltage between 15 and 110 volts AC.

The analysis reveals that the conditions at sound onset are 60 volts and 0.37 amps for a power requirement of 22 watts. Sound could be maintained at 45 volts and 0.27 amps for a power requirement of 12 watts. These results are the average of three sets of voltage measurements, and amperage is derived from the heat band curve. These results (22 watts and 12 watts) are significantly lower than the power requirements reported by Buda-Ortins (44 watts and 34 watts). It would appear that in addition to the lower temperature requirement brought about by the introduction of water, there is also a reduction in the required power input. As the heat transfer analysis will show, the reduction in power input has a significant impact on the feasibility of the device.

6 Heat Transfer Analysis

For the duration of prototype testing, the power source consisted solely of an electric heat band. A heat band was used for simplicity and precise control over the input power; however, the final form of the device would ostensibly be powered entirely by radiant energy from an emissive smoke layer. To accomplish this, a series of connected systems needs to be designed to capture the radiation from the smoke layer, convert the radiation to heat with a specified temperature and power level, and channel that heat into the device via the hot heat exchanger. To that end, a series of collectors and heatpipes were implemented, the details of which are outlined below.

6.1 Overview of Collector / Heatpipe System

In order to collect the radiant heat from the smoke layer, rectangular copper plates are oriented parallel to the smoke layer such that one side receives the maximum possible amount of thermal radiation. The upward facing side is also painted black with highly emissive grill paint ($\varepsilon = 0.99$) to maximize absorption. In addition to enhancing heat transfer, this allows for a black body assumption in the heat transfer calculations. The physical mechanism behind the operation of these "collectors" is as follows: As a compartment fire moves past its incipient stages, a hot smoke layer begins to form near the ceiling. The emissivity of the smoke layer is determined by its optical density (typically a characteristic property of the fuel) and the path length. As the smoke layer thickens, the path length increases until the smoke layer can be reasonably approximated as a black body. The changing kinetic

energies of the atoms and molecules in the smoke cause the production of wide-spectrum electromagnetic radiation. Some fraction of the emitted radiation reaches the collector, and a small amount of that is reflected. The remaining radiation is absorbed in a process that converts the photons into kinetic energy, raising the average temperature of the receiving object. The sizing process for the collectors is the subject of the succeeding section: "Extended Surface Analysis."

Once the requisite energy is stored in the collector panels in the form of heat, the objective becomes moving that energy from the collector panels to the hot heat exchanger. Due to the geometric arrangement of the collector apparatus and the design that places the collector panels on the outside of the helmet, there is a minimum distance of about 4 inches between the panels and the device. This distance precludes simple conduction as the mechanism of heat transfer between the panels and device; conduction is simply too slow and the thermal resistance of conductive solids too great to achieve the desired effect. The solution to this problem is a unique heat transfer device known as a heat pipe.

A heat pipe is a device that effects heat transfer by taking advantage of thermal conductivity as well as phase transition. It consists of a conductive casing, a wick, and a vapor cavity. A variety of materials are used for the conductive casing, but copper is by far the most common and readily available. The wick structure usually consists of a sintered metal powder or a series of parallel grooves, but can be anything that exerts capillary pressure on the liquid phase of the working fluid. The vapor cavity is a variable pressure cavity that contains a small amount of

working fluid. The cavity pressure and the composition of the working fluid are chosen to provide optimal performance at the desired temperature range.

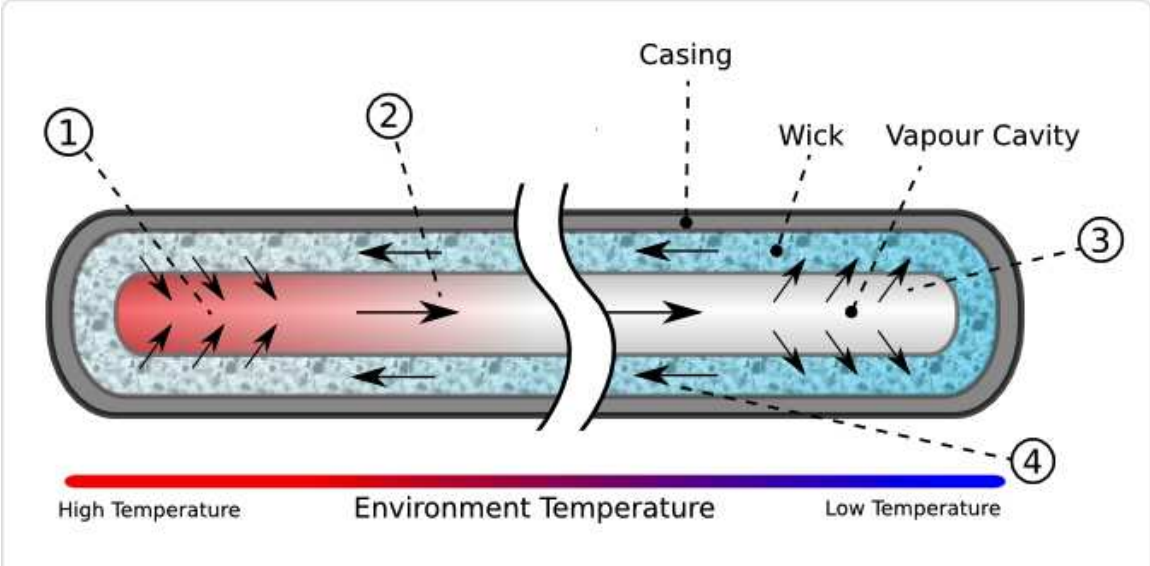

Figure 6-1: Heat pipe and heat flow diagram. [16]

One end of the heat pipe is placed in a high temperature environment and the other in a low temperature environment. This is often accomplished by soldering the ends of the heat pipe to the hot and cold objects. Heat from the hot environment enters the hot side of the heat pipe through the conductive casing. Heat moves from the hot side of the heat pipe to the cold side in two ways: by conduction along the axis of the pipe and by phase transition. The working fluid evaporates on the hot side of the heat pipe, absorbing the heat of vaporization, and condenses on the cold side of the heat pipe, depositing the heat of vaporization. The heat that is deposited on the cold side is then conducted out of the heat pipe by conduction through the casing. After condensing on the cold side, the liquid-phase working fluid moves back to the hot side by capillary action through the wick. The majority of the heat

transfer is accomplished through phase transfer, which offers resistance on an order of several magnitudes less than that of axial conduction.

The heat pipes used for this project were purchased from Advanced Cooling Technologies (ACT). They are 6-inches long (15.2cm) and made of copper, with water as the working fluid. The inner diameter of the heat pipes was 5mm and the wall thickness was 0.5mm, for an outer diameter of 6mm. The heat pipes were purchased prior to the establishment of temperature and power requirements for the purposes of investigation and collector design; therefore, they do not represent the final heat pipe selection and may need to be adjusted for sizing and temperature range.

For implementation into the collector apparatus, the edges of two collector plates are crimped and wrapped around the heat pipe as shown in *Figure 6-2.* The heat pipe was carefully bent into a curve with a 2-inch radius for future attachment to the thermoacoustic device.

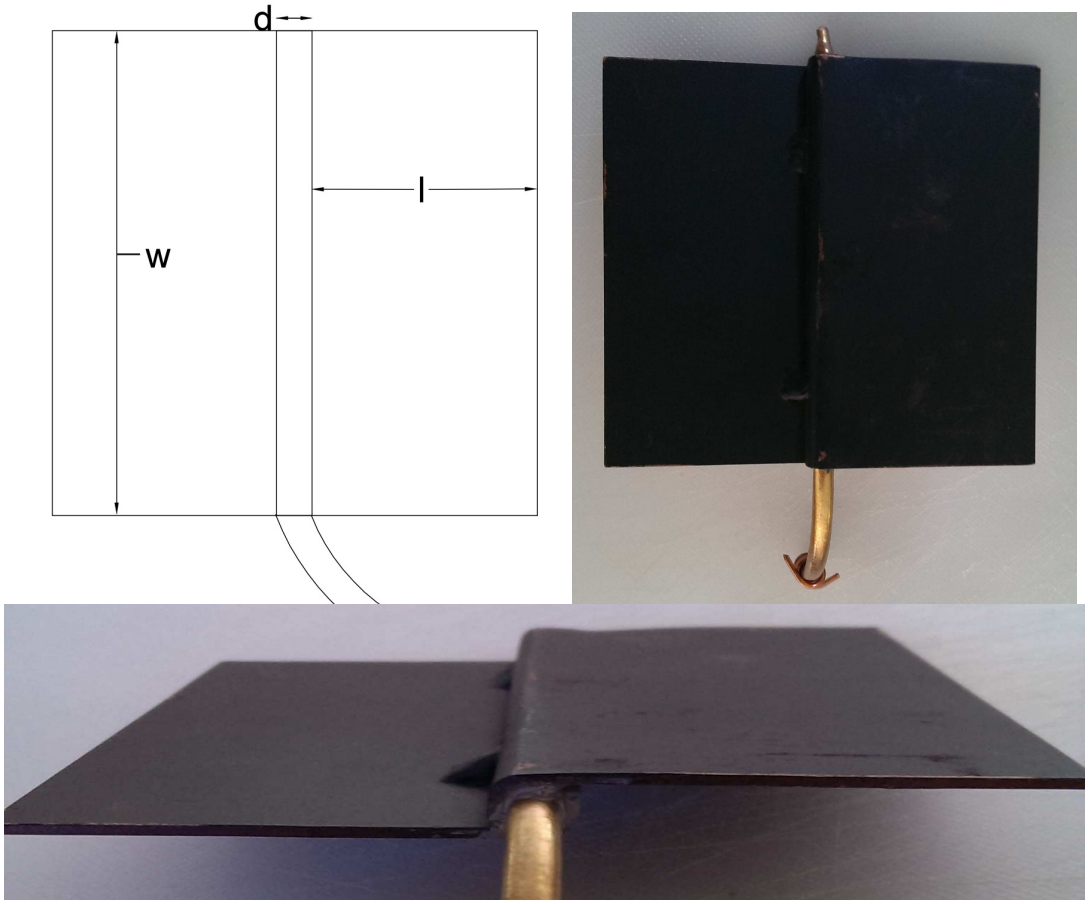

Figure 6-2: Diagram, top view, and side view of one collector panel with heat pipe.

6.2 Extended Surface Analysis

The sizing of the collector panels requires a heat transfer analysis of the source (smoke layer), collector, and heat pipe system. The function and structure of the collector panels qualify them as fins, or extended surfaces, which are widely studied for their applications in heating and cooling. An extended surface is used to increase the heat transfer from a surface by increasing the effective surface area. In this case, the collector panels extend from the heat pipe to capture more energy than the heat pipe would capture by itself. The equations derived below are an extended surface heat transfer analysis of the collector panels. First, an expression

for the temperature profile in the extended surface is derived, and then the temperature profile is used to perform an energy balance on the fin. The energy balance provides the relationship between all parameters needed to size the fin to capture the appropriate amount of energy.

Consider a control volume spanning the width and thickness of the collector with finite length. Let dx represent the length of the element extending in a direction perpendicular to the heat pipe. Let dw represent the width of the element extending in a direction parallel to the heat pipe. Due to symmetry about a line bisecting the heat pipe in contact with the collector, there is no net movement of heat in the direction parallel to the heat pipe. Additionally, the back of the panel (the side facing away from the smoke layer) is assumed to be heavily insulated, and therefore adiabatic. The energies entering and leaving the finite volume are shown in *Figure 6-3.*

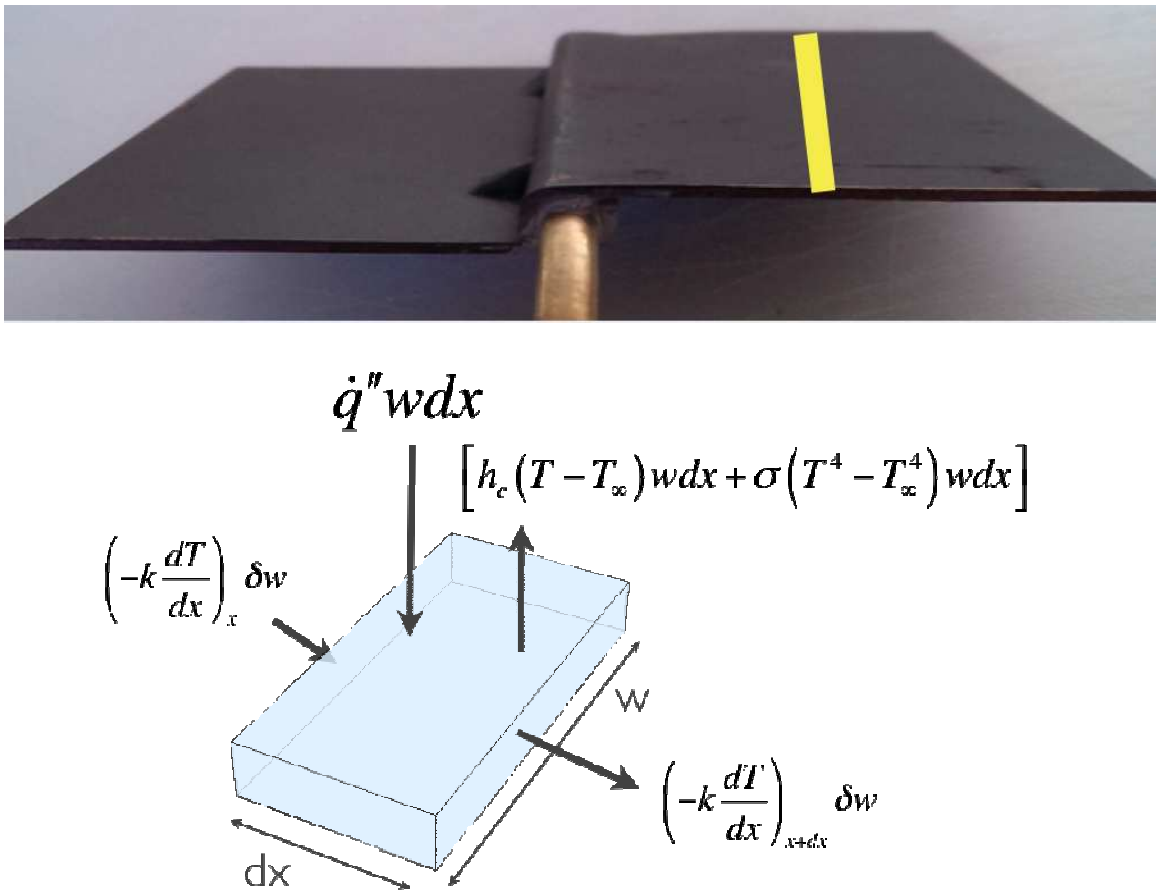

Figure 6-3: Control volume energy balance for extended surface.

$\dot{q}''$ is the radiant heat flux received by the control volume at the time of device activation. $\dot{q}''wdx$ is therefore the total amount of heat received by the control volume from the smoke layer. Heat is lost from the surface of the panel through radiation and convection. The convective losses are $h_c\left(T-T_\infty\right)wdx$ where h_c is a convection coefficient, T is the temperature of the control volume surface, and T_∞ is the ambient temperature. Radiation losses are given by $\sigma\left(T^4-T_\infty^4\right)wdx$, which is fairly conservative, as it assumes maximum losses to ambient surroundings. Heat moving through the extended surface perpendicular to the heat

pipe is transferred by conduction, and can be represented with Fourier's law. One side of the control volume receives $\left(-k\frac{dT}{dx}\right)_x \delta w$ where δ is the thickness of the panel, and $\left(-k\frac{dT}{dx}\right)_{x+dx} \delta w$ leaves through the opposite side. It is worth noting that this control volume analysis assumes that the collector panels receive radiation from the smoke layer, but that all convective activity is cooling. In physical terms, the assumption is that the firefighter's helmet will be below the bottom of the smoke layer, and surrounded by air at the ambient temperature.

The energy being conducted out of the element can be represented by the following Taylor series:

$$\left(-k\frac{dT}{dx}\right)_{x+dx} \delta w = \left[\left(-k\frac{dT}{dx}\right)_x + \frac{d}{dx}\left(-k\frac{dT}{dx}\right)dx\right]\delta w \qquad (1)$$

The energy balance on the control volume for steady state is then:

$$\dot{q}''wdx - \left[h_c\left(T-T_\infty\right)wdx + \sigma\left(T^4-T_\infty^4\right)wdx\right] + \left(-k\frac{dT}{dx}\right)_x \delta w - \left[\left(-k\frac{dT}{dx}\right)_x + \frac{d}{dx}\left(-k\frac{dT}{dx}\right)dx\right]\delta w = 0 \qquad (2)$$

And adding the conduction terms gives:

$$\dot{q}''wdx - \left[h_c\left(T-T_\infty\right)wdx + \sigma\left(T^4-T_\infty^4\right)wdx\right] - \left[\frac{d}{dx}\left(-k\frac{dT}{dx}\right)dx\right]\delta w = 0 \qquad (3)$$

The wdx term drops out, which yields:

$$\dot{q}'' - h_c\left(T-T_\infty\right) - \sigma\left(T^4-T_\infty^4\right) + \frac{d}{dx}\left(k\frac{dT}{dx}\right)\delta = 0 \qquad (4)$$

The $\sigma\left(T^4-T_\infty^4\right)$ term can be linearized to take the form:

$$\sigma\left(T^4-T_\infty^4\right) = \sigma\left(T^2+T_\infty^2\right)\left(T+T_\infty\right)\left(T-T_\infty\right) \qquad (5)$$

Additionally, if the following definitions are implemented:

$$h_r \equiv \sigma\left(T_0^2 + T_\infty^2\right)\left(T_0 + T_\infty\right) \qquad (6)$$

$$\text{and} \qquad \theta \equiv T - T_\infty \qquad (7)$$

the energy balance becomes:

$$\dot{q}'' - h_c\theta - h_r\theta + \frac{d}{dx}\left(k\frac{dT}{dx}\right)\delta = 0 \qquad (8)$$

Dividing *Equation 8* by $k\delta$, recognizing that $\frac{d\theta}{dx} = \frac{dT}{dx}$, and defining $h \equiv h_r + h_c$:

$$\frac{\dot{q}'' - h\theta}{k\delta} + \frac{d}{dx}\left(\frac{d\theta}{dx}\right) = 0 \qquad (9)$$

and if the following definitions and substitutions are implemented,

$$\phi \equiv \frac{\dot{q}'' - h\theta}{k\delta} \qquad (10)$$

$$\frac{d\phi}{dx} = -\frac{h}{k\delta}\frac{d\theta}{dx} \qquad (11)$$

$$\beta^2 \equiv \frac{h}{k\delta} \qquad (12)$$

the energy balance takes the final form:

$$\frac{d}{dx}\left(\frac{d\phi}{dx}\right) - \beta^2\phi = 0 \qquad (13)$$

This is a linear, second-order, homogenous differential equation whose analytical solution is: (see appendix B for verification)

$$\phi(x) = C_1\sinh(\beta x) + C_2\cosh(\beta x) \qquad (14)$$

$$\text{and} \qquad \frac{d\phi}{dx} = C_1\beta\cosh(\beta x) + C_2\beta\sinh(\beta x) \qquad (15)$$

Boundary conditions can be specified in terms of the base (collector) and tip of the fin.

Base Condition: $$\phi(0) = \frac{\dot{q}'' - h\theta_0}{k\delta} = \frac{\dot{q}'' - h(T_0 - T_\infty)}{k\delta} \qquad (16)$$

Adiabatic Tip Condition: $$\left.\frac{d\phi}{dx}\right|_{x=l} = 0 \qquad (17)$$

Using the boundary conditions to solve for the coefficients C_1 and C_2:

$$C_1 = -\phi_0 \frac{\sinh(\beta l)}{\cosh(\beta l)} \qquad (18)$$

$$\text{and} \quad C_2 = \phi_0 \qquad (19)$$

Equation 14 then becomes:

$$\phi(x) = -\phi_0 \frac{\sinh(\beta l)}{\cosh(\beta l)} \sinh(\beta x) + \phi_0 \cosh(\beta x) \quad (20)$$

which can be rearranged as follows:

$$\frac{\phi(x)}{\phi_0} = \frac{\cosh(\beta x)\cosh(\beta l) - \sinh(\beta l)\sinh(\beta x)}{\cosh(\beta l)} \qquad (21)$$

Using the following hyperbolic function identity:

$$\cosh(x - y) = \cosh(x)\cosh(y) - \sinh(x)\sinh(y) \qquad (22)$$

Equation 21 can be rearranged to take its final form:

$$\frac{\phi(x)}{\phi_0} = \frac{\cosh[\beta(l - x)]}{\cosh(\beta l)} \qquad (23)$$

Equation 23 provides an expression for the non-dimensional temperature profile of the fin as a function of x, or the direction perpendicular to the heat pipe. This

expression will be used in the collector energy balance to calculate the losses from the surface of the panel.

The steady-state energy balance accounts for the total energy entering and leaving the collector. The analysis accounts for half of a collector; that is, one copper plate and half of the heat pipe (each heat pipe is served by two copper plates). The energy that enters the panel through the surface directly over one half of the heat pipe is $\dot{q}''w\frac{d}{2}$ where d is the diameter of the heat pipe. The energy losses over the heat pipe due to convection are given by $h_c\left(T_0-T_\infty\right)w\frac{d}{2}$ where T_0 is the temperature of the extended surface at the position of the heat pipe (x=0). The losses over the heat pipe due to radiation are given by $\sigma\left(T_0^4-T_\infty^4\right)w\frac{d}{2}$. The energy carried from the heat pipe to the device is denoted $\dot{q}_p$, and so the energy carried from each individual plate is $\frac{\dot{q}_p}{2}$. The energy that enters the extended surface from beyond the heat pipe is given by $\int_0^L \dot{q}''w\,dx$ and the losses are given by $\int_0^L \dot{q}_l''w\,dx$ for a heat loss of $\dot{q}_l''$.

The collector energy balance is therefore:

$$\left[\dot{q}''-h_c\left(T_0-T_\infty\right)-\sigma\left(T_0^4-T_\infty^4\right)\right]w\frac{d}{2}-\frac{\dot{q}_p}{2}+\int_0^L\left[\dot{q}''-\dot{q}_l''\right]w\,dx=0 \qquad (24)$$

The heat lost from the extended surface, $\dot{q}_l''$, can be defined as follows:

$$\dot{q}_l''\equiv h\left(T-T_\infty\right) \qquad (25)$$

where h is the combined heat transfer coefficient, and T is the temperature at any point on the extended surface. T, and therefore $\dot{q}_l''$, are functions of x.

The term $\int_0^l [\dot{q}'' - \dot{q}_l''] w\, dx$ can be evaluated as follows:

$$\int_0^l [\dot{q}'' - \dot{q}_l''] w\, dx = w \int_0^l \left[\dot{q}'' - h\left(T - T_\infty\right)\right] dx \qquad (26)$$

and by our earlier definition in *Equation 10*, $T - T_\infty = -\frac{\phi k \delta}{h} + \frac{\dot{q}''}{h}$, and substituting into E*quation 26*:

$$w \int_0^l \left[\dot{q}'' - h\left(T - T_\infty\right)\right] dx = w \int_0^l \left[\dot{q}'' - h\left(-\frac{\phi k \delta}{h} + \frac{\dot{q}''}{h}\right)\right] dx \qquad (27)$$

Simplifying the right-hand side:

$$w \int_0^l \left[\dot{q}'' - h\left(-\frac{\phi k \delta}{h} + \frac{\dot{q}''}{h}\right)\right] dx = w \int_0^l [\phi k \delta]\, dx = wk\delta \int_0^l [\phi]\, dx \qquad (28)$$

Using our solution to the differential equation:

$$wk\delta \int_0^l [\phi]\, dx = wk\delta \int_0^l \left[\phi_0 \frac{\cosh[\beta(l-x)]}{\cosh(\beta l)}\right] dx = \frac{wk\delta\phi_0}{\cosh(\beta l)} \int_0^l \left[\cosh[\beta(l-x)]\right] dx \qquad (29)$$

Evaluating the integral yields:

$$\frac{wk\delta\phi_0}{\cosh(\beta l)} \int_0^l \left[\cosh[\beta(l-x)]\right] dx = \frac{wk\delta\phi_0 \sinh(\beta l)}{\beta \cosh(\beta l)} = \frac{wk\delta\phi_0}{\beta} \tanh(\beta l) \qquad (30)$$

Substituting *Equation 30* back into the collector energy balance (*Equation 24*) yields:

$$\left[\dot{q}'' - h_c\left(T_0 - T_\infty\right) - \sigma\left(T_0^4 - T_\infty^4\right)\right] w \frac{d}{2} - \frac{\dot{q}_p}{2} + \frac{wk\delta\phi_0}{\beta} \tanh(\beta l) = 0 \qquad (31)$$

Multiplying by 2 and dividing by wd gives the final form of the solution:

$$\left[\dot{q}'' - h_c\left(T_0 - T_\infty\right) - \sigma\left(T_0^4 - T_\infty^4\right)\right] - \frac{\dot{q}_p}{wd} + \frac{2k\delta\phi_0}{\beta d}\tanh\left(\beta l\right) = 0 \qquad (32)$$

Equation 32 is the expression that relates the size of the panel (w, l, and δ) to the critical onset heat flux ($\dot{q}''$) and environmental conditions (h_c, T_∞). The only remaining unknown is T_0, the steady-state temperature at the base of the collector. To determine T_0, a resistance analogy is applied between the cold end of the heat pipe and the base of the collector. In general, the resistance analogy is $R_{tot} = \sum R_t = \frac{\Delta T}{q}$ [17]. In the case of the collector heat pipe system, ΔT is the difference between the collector base temperature and the cold end of the heat pipe, or $T_0 - T_{HP}$. It is important to note that the cold end of the heat pipe is still the hottest part of the whistle. To avoid confusion, the hot side of the heat pipe at the collector base will be denoted with subscript "0", and the cold side will be denoted with subscript "HP." q is $\dot{q}_p$, or the energy moving through the heat pipe. The required temperature at the cold of the heat pipe (T_{HP}) is analogous to the sound-onset temperature of the heat band, which has been determined experimentally; Buda-Ortins found it to be $308^\circ C$, but with the addition of water, it was brought as low as $285^\circ C$. A conservative estimate for the temperature needed at the cold end of the heat pipe is $300^\circ C$. The thermal resistances relevant to the system are shown in *Figure 6-4.*

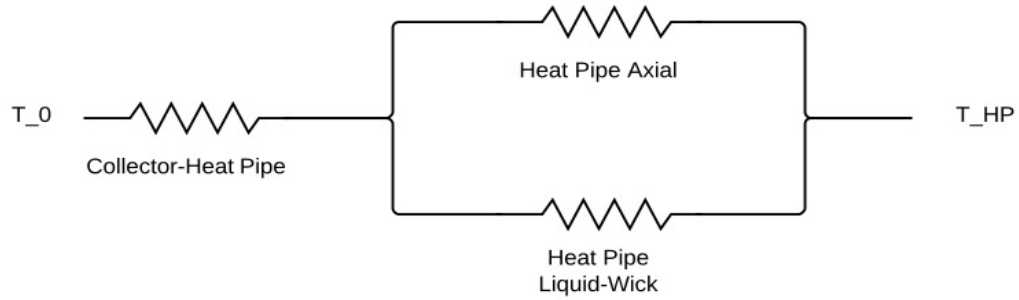

Figure 6-4: The resistance analog shown as a circuit diagram for the collector-heat pipe system.

The resulting analogy is:

$$R_{collector-heatpipe} + \frac{1}{\frac{1}{R_{heatpipe-axial}} + \frac{1}{R_{heatpipe-liquidwick}}} = \frac{T_0 - T_{HP}}{\dot{q}_p} \tag{33}$$

or in terms of T_0:

$$T_0 = \dot{q}_p \left[R_{collector-heatpipe} + \frac{1}{\frac{1}{R_{heatpipe-axial}} + \frac{1}{R_{heatpipe-liquidwick}}} \right] + T_{HP} \tag{34}$$

The first resistance met as the energy travels through the system is between the base of the collector and the heat pipe. Although the crimped edges of the plates make fairly good contact with the heat pipe, the thickness of the plates prevents perfect contact. The actual contact is more similar to what is shown on the left side of *Figure 6-5.*

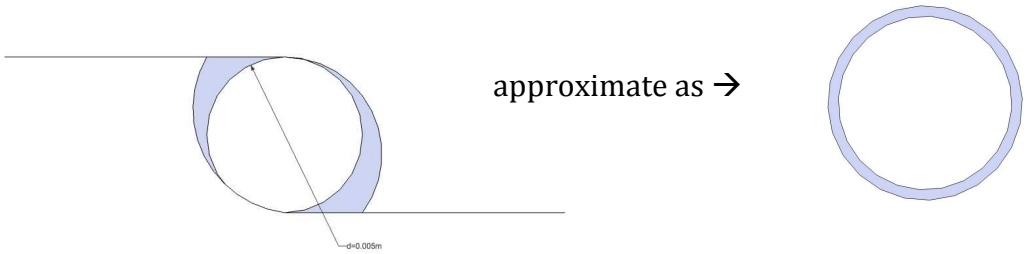

Figure 6-5: The gap between the collector plates and the heat pipe surface can be approximated as uniform concentric circles.

To estimate the resistance offered by this interface, the non-uniform contact between the plates and the heat pipe is approximated instead as concentric circles, shown on the right side of *Figure 6-5.* This resistance can then be calculated as [17]:

$$R_{collector-heatpipe} = \frac{l}{kA} \qquad (35)$$

where l is the path length of the traveling energy, k is the coefficient of conduction, and A is contact area. Based on the average gap width, l can be approximated as $0.5mm$. To improve conduction in the gaps between the plates and the heat pipe, small bits of copper wire and conductive paste were inserted in the gap. Due to the gap's small size, ensuring uniform application of the paste was difficult. For a conservative estimate, the conduction of the gap was approximated as that of air, or $0.05 {}^{W}\!/_{mK}$. The area of contact is given by $A = w(d + 2l)\pi$.

The next resistance met is that of the heat pipe. In Peterson's book on heat pipes, he lists the following resistances and their orders of magnitude. [18]

Resistance Type	Order of Magnitude
Liquid-wick resistance in the adiabatic section	10^4
Axial resistance of the pipe wall	10^2
Liquid-wick resistance in the evaporator	10^1
Liquid-wick resistance in the condenser	10^1
Radial resistance of the pipe wall at the evaporator	10^{-1}
Radial resistance of the pipe wall at the condenser	10^{-1}

Table 6-1: The thermal resistances offered by a heat pipe and their respective magnitudes.

Peterson offers a formula for calculated the liquid-wick resistance in all three sections of the heat pipe (evaporator, adiabatic, and condenser). The formula is:

$$R_{heatpipe-liquidwick} = \frac{\ln(d_o / d_i)}{2\pi L K_{eff}} \qquad (36)$$

where $K_{eff} = \varepsilon k_l + k_w(1-\varepsilon)$, and k_l is the coefficient of conduction for the liquid-phase working fluid, k_w is the coefficient of conduction for the wick, and ε is the wick porosity. L is the length of the heat pipe, and d_o and d_i are the outer and inner diameters of the heat pipe, respectively. The axial resistance in the pipe wall is given by:

$$R_{heatpipe-axial} = \frac{l_{adiabatic}}{k_{shell}A} \quad (37)$$

where $\frac{l_{adiabatic}}{k_{shell}A}$ is the length of the heat pipe section between the evaporator and condenser. k_{shell} is the coefficient of conduction for the heat pipe casing, and A is the area of the heat pipe walls.

A set of example values that result from substituting *Equations 35, 36, and 37* into *Equation 34* are shown in the parametric table, *Table 6-2*:

$\dot{q}_p(Watts)$	$T_0(^\circ C)$	$T_0 - T_{HP}(^\circ C)$
1	305	5
2	310	10
3	316	16
4	321	21

Table 6-2: Variation in temperature difference across the heat pipes with varying power.

As *Equation 33* suggests, the temperature difference between the hot end and cold end of the heat pipe vary linearly with the power that it carries. Under the particulars of this system, every additional watt that the heat pipe is made to carry increases the temperature difference by about $5^\circ C$. If the thermoacoustic device requires $300^\circ C$ for activation, it must reach $280^\circ C$ above ambient temperatures.

Even under the stress of 4 watts, the temperature difference between the ends of a heat pipe only accounts for less than 10% of the temperature requirement.

As the parametric table shows, the decision of how many watts each heat pipe must supply to the device will dictate the temperature that the collector is required to reach. If the wattage required to power the device is known, the determining factor will be the number of heat pipes in use. Because the number of heat pipes is a fairly flexible design parameter, it will remain a parametric variable and the fin sizing process will be conducted for several heat pipe numbers. All that remain before *Equation 32* can be solved for the size of the collector are the "environmental" parameters $\left(\dot{q}'', h_c, T_\infty\right)$.

The choice of an activation incident heat flux, $\dot{q}''$, is fundamental to the successful operation of the device. Radiant heat flux is the primary mode of heat transfer to an inhabitant in an enclosure fire, especially given the assumption that the inhabitant is located beneath the smoke layer, so a threshold incident radiant heat flux is a reasonable choice of activating factor. Selecting the threshold requires careful analysis of incident floor heat flux and fire development. While definitions of flashover differ, it is often associated with high incident heat fluxes in the range of $20\,{kW}/{m^2}$. A prudent choice of alarm activation heat flux would be in the area of $10\,{kW}/{m^2}$. Although this represents only half the incident heat flux associated with flashover, it represents a much greater fraction of the time until flashover, as fire growth is generally non-linear. The driving force behind the radiant smoke layer is the heat release rate of the fire, which is often modeled with a t^2 growth pattern. If

a t^2 fire is a reasonable approximation, the heat release rate will reach half of its maximum value at a time of $t = \sqrt{\frac{1}{2}} t_{\max}$, or closer to 70% of the time to flashover. This leaves firefighters with approximately 30% of the time until flashover to escape from a compartment. Time until flashover varies with fuel load and compartment geometry, but research performed by Babrauskas et al [19] gives the time until flashover of a room with plywood walls, GWB ceiling, and mixed furniture as between 100 and 120 seconds. This represents escape times of approximately 30-36 seconds.

Equation 32 is not trivial to solve due to its hyperbolic function. A MATLAB program was written to solve *Equation 32* for the length of the collector panels by finding the zeroes of the function to a prescribed degree of precision. The program can be found in Appendix C.

The required length of the collector plates is shown as a function of the T_{HP} temperature in *Figure 6-6*. Each series in *Figure 6-6* represents a separate heat pipe configuration that differs in the amount of power each heat pipe must carry. The amount of power that the heat pipes must carry is determined by the total power requirement of the device and the number of heat pipes attached to the device. The range of the plot is only the length of one collector plate; the total length of the panel is $2l + d$, as each panel is made up of two plates on either side of a heat pipe. The information in *Figure 6-6* is applied to the experimental model and the results are shown in *Figure 6-7,* which gives the total collector area for the optimized prototype, with selected inputs of 22 watts and $300^{\circ}C$, as a function of the number of heat

pipes in use. The inputs chosen for this analysis come directly from the experimental results of the optimization work, and are conservative design estimates. The total collector area is calculated as $n_{pipes} w(2l+d)$. The total area is essentially a measure of relative efficiency; if a greater number of heat pipes require a lower total area, each extended surface is delivering more power per unit area. This quantity is an important design parameter, because it is an indicator of feasibility. If the total design area exceeds the available area on the surface of a firefighting helmet, the design is impractical.

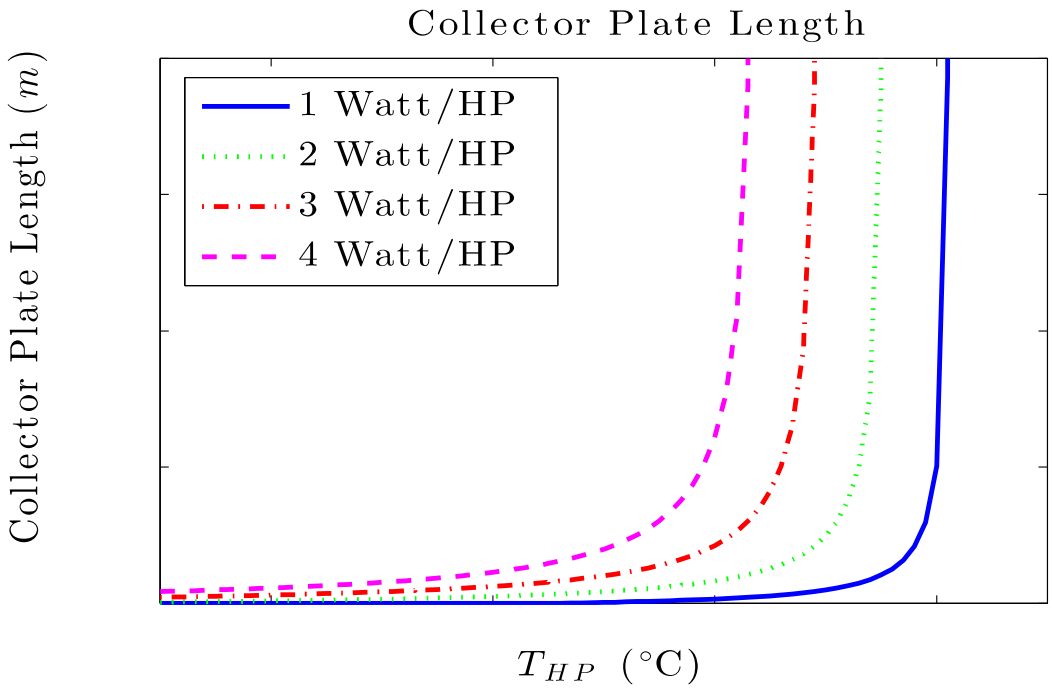

Figure 6-6: Collector plate length as a function of THP for various configurations.

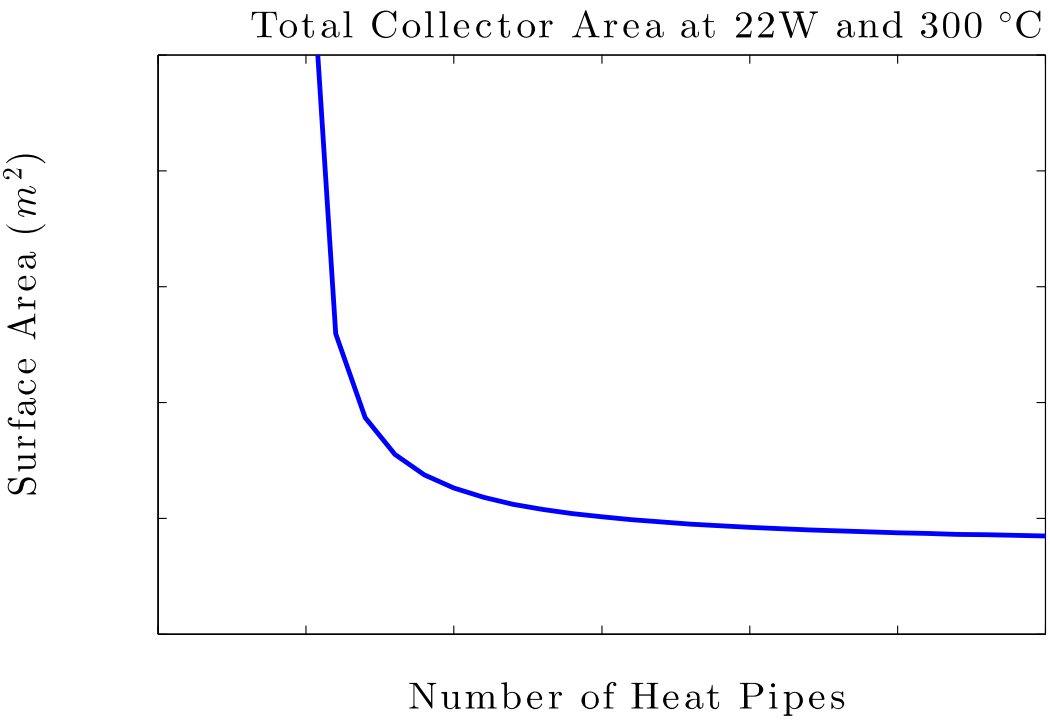

Figure 6-7: Total collector area for a design requiring 22W and 300C as a function of heat pipe quantity.

The behavior of the collector panels is similar across all power requirements. For a range of relatively low temperatures, the required length of the collector plates increases in a fairly linear fashion. As the required temperature increases, the collector lengths grow exponentially, rapidly becoming infinite as the temperature reaches its maximum value. Above that temperature, the bounds of the cosh function are exceeded, and the equation returns negative length values. In physical terms, this represents the extended surface losing efficiency as its length grows. When the lengths are small, the temperatures achieved are lower. This reduces energy loss from the panel, allowing a higher percentage of input heat to flow into the heat pipe. When higher temperatures are necessary, the length of the panels must grow accordingly; however, higher temperatures lead to higher losses,

and longer panels mean a longer path for the heat to travel. The result is a reduction in collector efficiency.

When the equations are reorganized to account for the total collector area in the specific case of a device requiring 22 watts and $300^{\circ}C$, the results show a massive area for a design with fewer than six heat pipes, which decreases rapidly until about 10 heat pipes, and then decreases only slightly more as the number of heat pipes is further increased. Because of behavior of this function, it is imperative that the choice of number of heat pipes keeps the total area in its pseudo-linear region. Fifteen heat pipes seems to be an ideal design, as it represents the fewest number of heat pipes that lies squarely in the pseudo-linear region of the plot, and provides a good balance of simplicity and efficiency. The use of fifteen heat pipes represents a required surface area of $0.02m^2$. If a future design were to place a premium on simplicity, ten heat pipes is still feasible, and represents a required surface area closer to $0.025m^2$.

6.3 Collector Response Time

In addition to the size of the collector panels, the response time is of interest as well. The purpose of the device is to warn firefighters of deteriorating conditions; if the device takes several minutes to reach the temperature and power levels it needs to begin whistling, it is useless. Assuming a lumped capacitance model as a first-order approximation, the governing equation is:

$$mc\frac{dT}{dt} = \left[\dot{q}'' - h\left(T - T_{\infty}\right)\right]A_s - \dot{q}_p \qquad (38)$$

where $h \equiv h_c + \sigma\left(T^2 + T_\infty^2\right)\left(T + T_\infty\right)$. Substituting $A_s = w\left(d + 2l\right)$ and $m = \rho\delta w\left(d + 2l\right)$:

$$\rho\delta w\left(d + 2l\right)c\frac{dT}{dt} = \left[\dot{q}'' - h\left(T - T_\infty\right)\right]w\left(d + 2l\right) - \dot{q}_p \qquad (39)$$

Dividing all terms by $w\left(d + 2l\right)hT_\infty$ to cancel out the area term and non-dimensionalize the temperature terms yields:

$$\frac{\rho\delta c}{hT_\infty}\frac{dT}{dt} = \left[\frac{\dot{q}''}{hT_\infty} - \frac{\left(T - T_\infty\right)}{T_\infty}\right] - \frac{\dot{q}_p}{hT_\infty w\left(d + 2l\right)} \qquad (40)$$

$$\frac{\rho\delta c}{T_\infty h}\frac{dT}{dt} = \left[\frac{\dot{q}''}{T_\infty h} - \left(\frac{T - T_\infty}{T_\infty}\right)\right] - \frac{\dot{q}_p}{T_\infty hw(d + l)}$$

The following definitions are implemented:

$$\theta \equiv \frac{T - T_\infty}{T_\infty} \qquad (41)$$

$$\tau \equiv \frac{th}{\rho c\delta} \qquad (42)$$

$$Q \equiv \frac{\dot{q}'' - \dot{q}_p \big/ w\left(d + 2l\right)}{hT_\infty} \qquad (43)$$

Substituting *Equations 41-43* into *Equation 40* gives the linear first-order differential equation:

$$\frac{d\theta}{d\tau} + \theta = Q \qquad (44)$$

whose solution is of the form:

$$\theta = Q\left(1 - e^{-\tau}\right) \qquad (45)$$

Taking a time constant, τ, of 1, the response of the collector is:

$$t_{response} = \frac{\rho c \delta}{h} \quad (46)$$

Response times for common materials and thicknesses are shown in *Table 6-3*.

Material	$\delta(in)$	$\rho\left(g/cm^3\right)$	$c\left(J/gK\right)$	$t_{response}(s)$
Copper	1/16	8.93	0.39	172.9
Copper	1/32	8.93	0.39	86.44
Brass	1/16	8.5	0.38	160.3
Brass	1/32	8.5	0.38	80.17
Aluminum	1/16	2.712	0.91	122.5
Aluminum	1/32	2.712	0.91	61.25

Table 6-3: Response time analysis for various material choices for collector plates and thicknesses.

Although copper seems to deliver the slowest and least desirable response time, the response times of all elements in *Table 6-3* are of an identical order of magnitude, and none of them are inherently incapable of producing sound within the desired time frame. Despite being the slowest to respond, copper remains the best option, due to its thermal conductivity. When the thermal conductivity of brass or aluminum is used in the preceding heat transfer analysis, the fins become impossibly large and thick in order to conduct sufficient energy to the heat pipes.

7 Acoustic Output Analysis and Practicality

Sound intensity is typically expressed on a logarithmic scale, with units of decibel SPL (sound power level), denoted "dB". The relationship between sound intensity and perceived loudness is shown in *Table 7-1*. [20]

$Watts / cm^2$	**Decibels SPL**	**Example Sound**
10^{-2}	140 dB	Pain
10^{-3}	130 dB	
10^{-4}	120 dB	Discomfort
10^{-5}	110 dB	Jack hammers / rock concert
10^{-6}	100 dB	Motorcycle
10^{-7}	90 dB	OSHA limit for industrial noise
10^{-8}	80 dB	Garbage disposal
10^{-9}	70 dB	Vacuum cleaner
10^{-10}	60 dB	Normal conversation
10^{-11}	50 dB	
10^{-12}	40 dB	Weakest audible at 100 Hz
10^{-13}	30 dB	
10^{-14}	20 dB	Weakest audible at 10kHz
10^{-15}	10 dB	
10^{-16}	0 dB	Weakest audible at 3 kHz
10^{-17}	-10 dB	
10^{-18}	-20 dB	

Table 7-1: Decibel power level and perceived loudness. [20]

The weakest sound detectable by the human ear is approximately 0 dB, or a sound wave power of 10^{-16} $Watts / cm^2$. 140 dB represents sound that is painfully loud. The Occupational Safety and Health Administration regulates permissible noise exposure in the workplace, and the maximum duration and hours and associated decibel levels are shown in the *Table 7-2*. [21]

Duration per day (hours)	Sound Level (dB)
8	90
6	92
4	95
3	97
2	100
1.5	102
1	105
0.5	110
0.25 or less	115

Table 7-2: OSHA maximum workplace noise exposure. [21]

Although not necessarily binding, the OSHA standard is good indicator of what might constitute an acceptable alarm volume for firefighters in the workplace. The expected duration of a flashover warning device falls well within the "0.25 hours or less" category, as the alarm is only designed to warn of imminent flashover occurring within 2-3 minutes or sooner. 115 dB is therefore a safe and reasonable maximum sound level parameter. A minimum sound level parameter is more difficult to determine, as setting it too low may result in a firefighter's inability to hear the alarm. When discussing alarm and notification sound levels, NFPA 72 [22] requires that alarms be 15 dB above average ambient sound levels or 5 dB above maximum ambient sound levels, whichever is greater. A typical structure fire will have (at a minimum) several diesel trucks in high idle surrounding the building and radio traffic (~75 dB). Using NFPA's standard as a relevant guide, a prudent minimum flashover alarm sound level would be about 90 dB.

The range of human hearing is generally considered to be 20 Hz to 20 kHz, but it is far more sensitive to sounds between 1 kHz and 4 kHz. Sensitivity, in this context, is measured by the lowest sound level at which a human can perceive any

given frequency. For example, listeners can detect sounds as low as 0 dB at 3 kHz, but require 40 dB at 100 Hz. The auditory response area over a range of frequencies is shown in the human audiogram in *Figure 7-1*. [23]

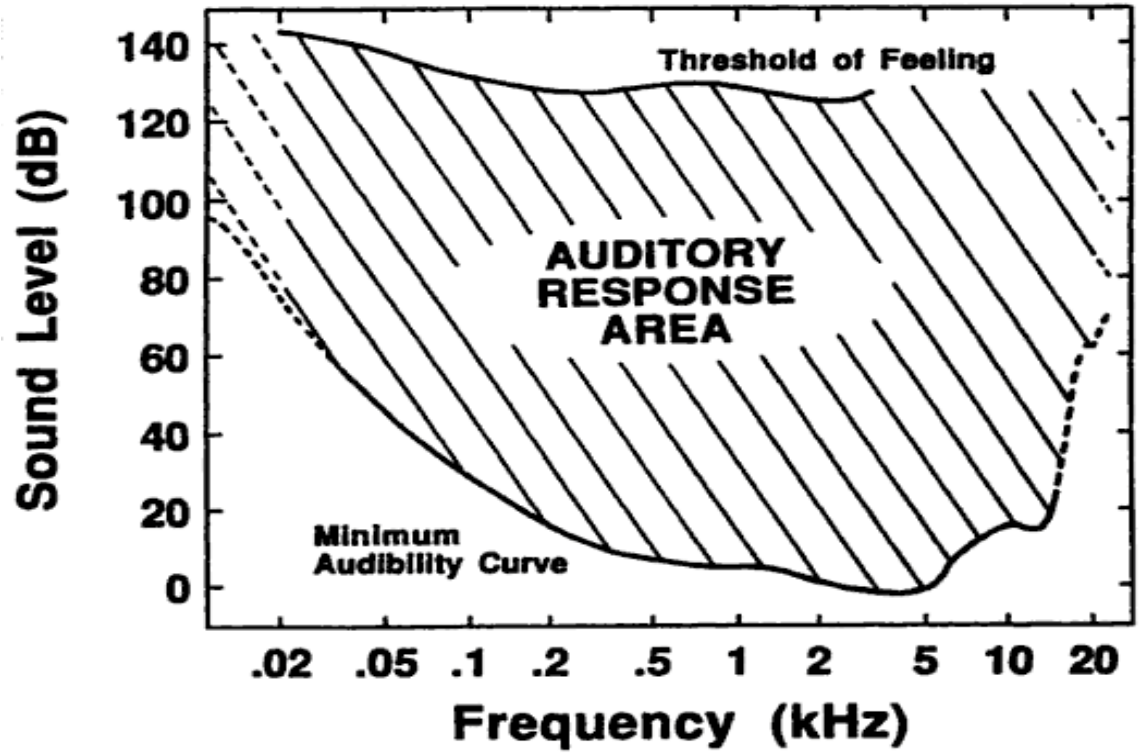

Figure 7-1: Human audiogram. [23]

It is clear that the lowest sound levels required for auditory perception exist between about 0.5 kHz and 6 kHz, with the absolute lowest point occurring at about 4 kHz. For the purposes of a flashover alarm, a frequency between 500 Hz and 6 kHz would be in an acceptable range, although a frequency closer to 4 kHz would be ideal.

Human listeners have the ability to discern the direction from which a sound originated, and to a more limited extent, the distance from which the sound originated. Although directionality is primarily determined by the difference in

signal strength between the right and left ears, research conducted by Sandel et al. [24] indicates that human subjects have the most difficulty localizing sinusoidal sound waves with frequencies between 1.5 and 3 kHz. Distance information is inferred from frequency, as sound waves tend to dissipate their higher frequencies as they propagate long distances. For this particular application of an acoustic alarm, the ability to localize the source of sound would be helpful, but not critical. The alarm will be mounted in a fixed position relative to the firefighters' ears, so localization is unimportant in identifying one's own alarm; however, it may be useful for firefighters to be capable of discerning the location of their partner's alarm for the purposes of situational awareness and rescue. If they can be easily avoided, frequencies between 1.5 and 3 kHz will not be used.

An acoustic analysis was performed on the prototype device using digital signal processing software (Audacity) and a HHSL402SD sound level meter. The frequency breakdown shows volume peaks at over a range of frequencies. The loudest peak occurs at just above 500 Hz, and represents most of the sound that is heard when the device is whistling. Secondary peaks occur at intervals of about 500 Hz (the fundamental mode that corresponds with the length of the device). The device puts out 101 dB of sound measured at a point 70mm from the open end of the device.

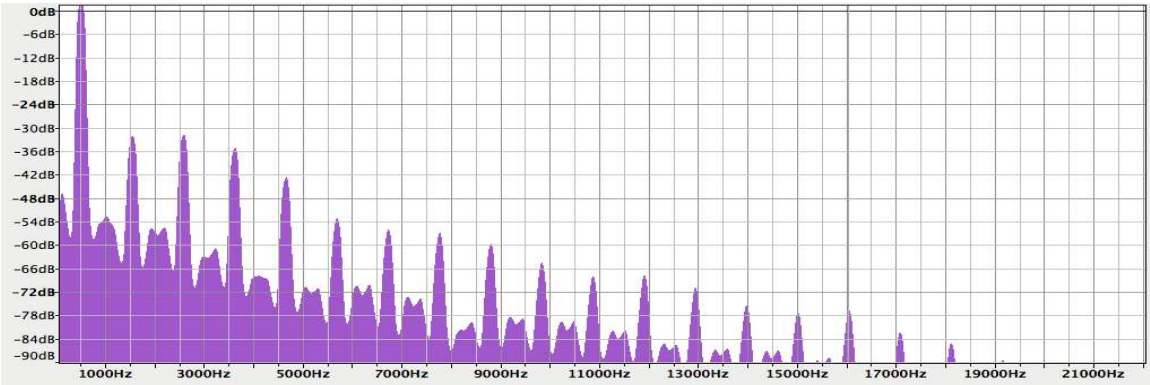

Figure 7-2: Sound analysis of device's whistling using "Audacity" audio processing software.

8 Conclusions and Suggestions for Future Work

Two related paths of research, prototype optimization and heat transfer analysis, were conducted in parallel. As such, conclusions from each affect the other, and future research should consider them in concert. The results of the prototype optimization were largely unproductive, as almost all of the modifications failed to produce sound. However, the failure of particular modifications does suggest future avenues for investigation. Decreasing the size of the prototype components had the opposite effect of what had been intended. Although increasing the size of the device is not particularly desirable, as a large device is difficult to incorporate inconspicuously into a helmet, it is possible that a slightly larger diameter could drastically decrease the temperature and power requirements.

The most successful attempt at optimization was the addition of water, which lowered the temperature by $23^{\circ}C$ and the power requirements by 12 watts. Although water had to be added manually to the prototypes during the assembly process for each testing cycle due to evaporation, there are a number of potential ways to incorporate phase-change liquids into a commercial version of this device, which present more possibilities for future research. One way would be to use a water gel, or water-absorbing polymer. The water would stay trapped in the solid until heated to a temperature just below the critical onset temperature. Once the critical onset temperature was reached, the liquid water would be available for vaporization. This type of solution would preclude the device from multiple instance of use, however, and the polymer would need to be replaced periodically.

The results of the prototype testing are used in the heat transfer analysis to determine the size of the collector panels. The model that incorporates water provides the most favorable conditions for activation, and a conservative design would provide 30 watts and $300^{\circ}C$. The total area required for activation under these conditions is approximately $0.05m^2$. This surface area teeters on the edge of feasibility; if it is possible to find $0.05m^2$ of upward-facing surface area on a helmet, it will be just barely so. If the water proves impossible to incorporate into the final design, measurements taken by Buda-Ortins dictate a design of 40 watts and $320^{\circ}C$. Even with 30 heat pipes, this design requires $0.1m^2$, which will almost certainly not be available. In the event that it is available, an object with a temperature of $300^{\circ}C$ is very hot to keep in the vicinity of a firefighter's head and in a plastic helmet. Lowering the onset temperature of the device should be a priority for any future research. In addition to making the device safer to put inside a helmet, a lower onset temperature will reduce the total collector surface area.

9 Appendix A

Original foam ID: $0.0229m$
Original foam height: $0.0076m$
Area of copper foam is in contact with: $\pi DL = \pi(0.0229)(0.0076) = 5.47E-4m^2$

Weight of empty copper ring: $13.8g$
Weight of copper ring and copper foam: $16.4g$
Weight of copper foam: $16.4-13.8=2.6g$

Density of solid copper: $8960\,{kg}/{m^3}$
Volume of copper foam: $\frac{\pi D^2 L}{4} = \frac{\pi(0.0229)^2(0.0076)}{4} = 3.13E-6m^3$
Density of copper foam: $0.0026kg / 3.13E-6 = 830\,{kg}/{m^3}$
Relative density of copper foam: $830/8960 = 0.092$ or 9.2%

From the graph (provided by ERG Aerospace):
9.2% relative density at 20 PPI: $32\,{in^2}/{in^3} = 1260\,{m^2}/{m^3}$
Foam surface area: $(1260)(3.13E-6) = 0.004m^2$
Surface area ratio: $0.004/5.47E-4 = 7.3$

For a 14mm ID heat exchanger: ${54\,in^2}/{in^3} \rightarrow 12\%@40PPI$
For a 19mm ID heat exchanger: ${39\,in^2}/{in^3} \rightarrow 6\%@40PPI$

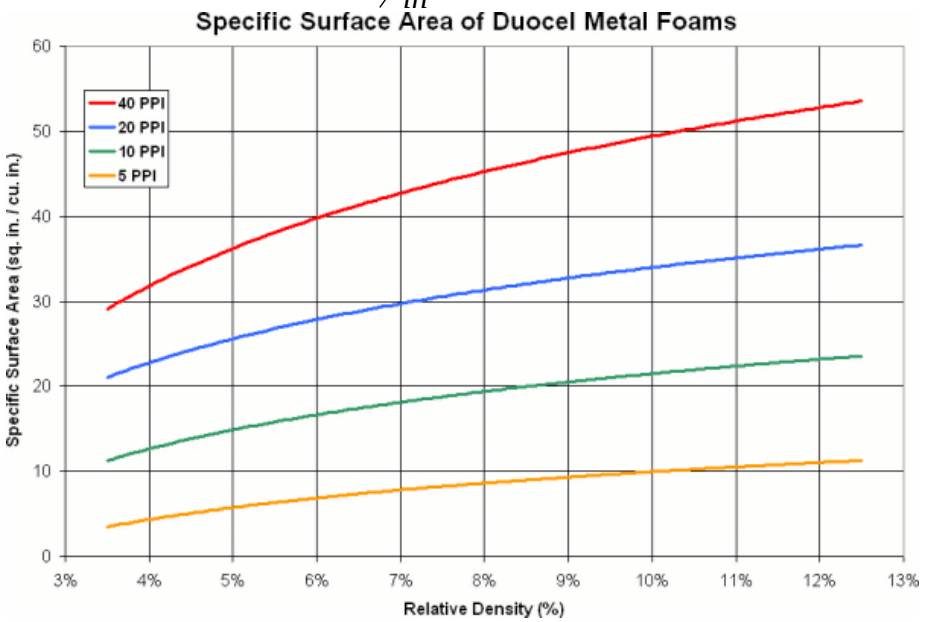

10 Appendix B

The second-order, homogenous, linear differential equation is:

$$\frac{d}{dx}\left(\frac{d\phi}{dx}\right)-\beta^2\phi=0$$

The solution is:

$$\phi(x)=C_1\sinh(\beta x)+C_2\cosh(\beta x)$$

$$\frac{d\phi}{dx}=C_1\beta\cosh(\beta x)+C_2\beta\sinh(\beta x)$$

Substituting the solution into the equation:

$$\frac{d}{dx}\left[C_1\beta\cosh(\beta x)+C_2\beta\sinh(\beta x)\right]-\beta^2\left[C_1\sinh(\beta x)+C_2\cosh(\beta x)\right]=0$$

Evaluating the derivative:

$$\left[C_1\beta^2\sinh(\beta x)+C_2\beta^2\cosh(\beta x)\right]-\beta^2\left[C_1\sinh(\beta x)+C_2\cosh(\beta x)\right]=0$$

Rearranging:

$$\beta^2\left[C_1\sinh(\beta x)+C_2\cosh(\beta x)\right]-\beta^2\left[C_1\sinh(\beta x)+C_2\cosh(\beta x)\right]=0$$

11 Appendix C

```
clear all

q_p_total=45; %W to run device
n_p=15; %number of heat pipes
q_p=q_p_total/n_p; %W heat pipe power


T_bottom=573; %K temperature of cold end of heat pipe
%properties of gap between collector and pipe
l_gap=0.0005;% m
k_gap=0.05;%W/mk thermal conductivity of air
A_gap=0.1*0.006*pi;%m^2 area of gap
R_collector_pipe=l_gap/(k_gap*A_gap);
R_axial=0.1/(400*pi*(0.0025^2-0.0015^2));
d_o=0.005;%m outer diameter of heat pipe
d_i=0.004;%m inner diameter of heat pipe
K_eff=0.5*0.5+0.5*400;
R_wick=log(d_o/d_i)/(2*pi*0.015*K_eff);
R_pipe=1/(1/R_axial+1/R_wick);
R_total=R_collector_pipe+R_pipe;
T_0=T_bottom+q_p*R_total; %relationship between T_0 and
T_bottom

w=0.1; %m length of evaporator
T_amb=293; %K ambient temperature
q=10000; %W/m^2 heat flux from ceiling
d=0.005; %m diameter of heat pipe
h_c=10; %W/m^2K convective heat transfer coefficient
deltainches=1/16; %in collector thickness
delta=.0254*deltainches; %m collector thickness
sigma=5.67E-8; %boltzmann constant
k=400; %W/mK conductivity of copper
h_r=sigma*(T_0^2+T_amb^2)*(T_0+T_amb);
h=h_c+h_r;
beta=sqrt(h/(k*delta));
theta_0=(q-h*(T_0-T_amb))/(k*delta);

%lower and upper bounds for parameter "l"
low=0;
high=1;

%iterative f(0) solver
for m=1:4

l=linspace(low,high,1001);

for x=1:1001
soln(x)=q-h_c*(T_0-T_amb)-sigma*(T_0^4-T_amb^4)-
q_p/(w*d)+2*k*delta*theta_0*tanh(beta*l(x))/(beta*d);
end
```

```
temp=abs(soln-0);
[idx idx]=min(temp);

middle=low+((idx-1)/1000)*(high-low);
newhigh=low+(idx/1000)*(high-low);
newlow=low+((idx-2)/1000)*(high-low);

high=newhigh;
low=newlow;
end

format long
length=middle
```

12 References

[1] Karter, Michael, and Joseph Molis. "US Firefighter Injuries - 2011." *NFPA* 1 (2012): 1-30. Print.

[2] Fahy, Rita, Paul LeBlanc, and Joseph Molis. "Firefighter Fatalities in the United States – 2011." *NFPA* 1 (2012): 1-36. Print.

[3] Karlsson, Björn, and James G. Quintiere. *Enclosure Fire Dynamics*. Boca Raton, FL: CRC Press, 2000. Print.

[4] *NFPA 1971, Standard on Protective Ensemble for Structural Fire Fighting*. 2000 ed. Quincy, MA: National Fire Protection Association, 2000. Print.

[5] Buda-Ortins, Krystyna. "Prototype Design of a Thermoacoustic Flashover Detector." *Master's Thesis* (2012): 1-96. Print.

[6] ISO Glossary of Fire Terms and Definitions, International Standards Organization, Geneva, 1996.

[7] Swift, G. W.. *Thermoacoustics: a Unifying Perspective for Some Engines and Refrigerators*. Melville, NY: Acoustical Society of America through the American Institute of Physics, 2002. Print.

[8] Knight, Randall. *Physics for Scientists and Engineers: a strategic approach*. San Francisco: Pearson/Addison Wesley, 2004. Print.

[9] Adapted from the Wikimedia Commons file "Thermo-acoustic cooling machine.png" http://en.wikipedia.org/wiki/File:Machine-thermoacoustique.png

[10] Jung, S and Matveev, K I, "Study of a small-scale standing-wave thermoacoustic engine," Journal of Mechanical Engineering Science, Vol. 224, 2009c.

[11] Wheatley, J., Hofler, T., Swift, G.W., Migliori, A., "Understanding some simple phenomena in thermoacoustics with applications to acoustical heat engines," American Journal of Physics, Vol. 53, pp. 147-162, 1985.

[12] Symko, O. G., Abdel-Rahman, Kwon, Y.S., Emmi, M., Behunin, R., "Design and development of high-frequency thermoacoustic engines for thermal management in microelectronics," Microelectronics Journal, Vol. 35, pp. 185-191, 2004.

[13] McLaughlin, Bonnie Jean. "Study and development of high-frequency thermoacoustic prime movers with piezoelectric transducers," Ph.D. Dissertation, The University of Utah, 2008.

[14] Smoker, J., Nouh, M., Aldraihem, O., Baz, A., "Energy harvesting from a standing wave thermoacoustic piezoelectric resonator," J. Appl. Phys. 111, 104901 (2012).

[15] Duocel Copper Foam. ERG Aerospace Corporation. [Online] 2011. http://www.ergaerospace.com/Copper-properties.htm.

[16] Adapted from the Wikimedia Commons file "Heat Pipe Mechanism.png" https://en.wikipedia.org/wiki/File:Heat_Pipe_Mechanism.png

Wikimedia Commons

[17] Incropera, Frank, and David DeWitt. *Fundamentals of Heat and Mass Transfer*. 3rd ed. New York: Wiley, 1990. Print.

[18] Peterson, G. P.. *An Introduction to Heat Pipes: Modeling, Testing, and Applications*. New York: Wiley, 1994. Print.

[19] Babrauskas, Vytenis, Peacock, Richard, and Rekene, Paul. *Defining Flashover for Fire Hazard Calculations: Part II*. Building and Fire Research Laboratory, NIST. (2003).

[20] Smith, Steven W. "Human Hearing." *The Scientist and Engineer's Guide to Digital Signal Processing*. San Diego, CA: California Technical Pub, 1997. N. pag. Print.

[21] *General industry: OSHA Safety and Health Standards (29 CFR 1910)*. Rev. Mar. 11, 1983. Washington, D.C.: U.S. Dept. of Labor, Occupational Safety and Health Administration, 1983. Print.

[22] *NFPA 72: National Fire Alarm and Signaling Code*. 2010 ed. Quincy, Mass.: The Association, 2009. Print.

[23] Rubel EW, Dobie RA: The auditory system: Central auditory pathways. In HD Patton, AF Fuchs, B Hille, AM Scher, R Steiner (ed.): Textbook of Physiology. Vol 1. 21st ed. Philadelphia: W. B. Saunders Company, 1989, pp 386-411.

[24] Sandel, T. T., Teas, D. C., Feddersen, W. E., Jeffress, L. A.: Localization of sound from single and paired sources. *Journal of the Acoustic Society of America.* 27:842-52.